A *trans*-acting long non-coding RNA represses flowering in *Arabidopsis*

Yu Jin[1], Maxim Ivanov[1], Anna Nelson Dittrich[2], Andrew D. L. Nelson[2] and Sebastian Marquardt[1*]

[*]Correspondence: sebastian.marquardt@plen.ku.dk

[1]Department of Plant and Environmental Sciences, Copenhagen Plant Science Centre, University of Copenhagen, Frederiksberg, Denmark

[2]Boyce Thompson Institute, Cornell University, Ithaca, NY, USA

Keywords

lncRNA, *FLAIL*, *trans*-acting, chromatin binding, flowering regulation, ChIRP-seq

Abstract

Eukaryotic genomes give rise to thousands of long non-coding RNAs (lncRNAs), yet the purpose of lncRNAs remains largely enigmatic. Functional characterization of lncRNAs is challenging due to multiple orthogonal hypothesis for molecular activities of lncRNA loci. Here, we identified a **fl**owering **a**ssociated **i**ntergenic **l**ncRNA (*FLAIL*) that represses flowering in *Arabidopsis*. An allelic series of *flail* loss-of-function mutants generated by CRISPR/Cas9 and T-DNA mutagenesis showed an early flowering phenotype. Gene expression analyses in *flail* mutants revealed differentially expressed genes linked to the regulation of flowering. A genomic rescue fragment of *FLAIL* introduced in *flail* mutants complemented gene expression defects and early flowering, consistent with *trans*-acting effects of the *FLAIL* RNA. Knock-down of *FLAIL* RNA levels using the artificial microRNA approach revealed an early flowering phenotype shared with genomic mutations, indicating a *trans*-acting role of *FLAIL* RNA in the repression of flowering time. Genome-wide detection of *FLAIL*-DNA interactions by ChIRP-seq suggested that *FLAIL* may directly bind genomic regions. *FLAIL* bound to genes involved in regulation of flowering that were differentially expressed in *flail*, consistent with the interpretation of *FLAIL* as a *trans*-acting lncRNA directly shaping gene expression. Our findings highlight *FLAIL* as a *trans*-acting lncRNA that affects flowering in *Arabidopsis*, likely through mediating transcriptional regulation of genes directly bound by *FLAIL*.

Background

The purpose of DNA sequences that do not encode proteins represents an open question in the biology of genomes. It is now clear that RNA polymerase II (RNAPII) converts non-coding DNA into non-coding RNA genome-wide [1]. Long non-coding RNAs (lncRNAs) are key products of ubiquitous RNAPII transcription in the non-coding genome [2]. Non-coding DNA engaged in lncRNA production may function through various molecular mechanisms, ranging from roles as DNA elements, RNAs, the act of transcription and small peptides [3, 4]. This wide range of possible cellular roles affects strategies to elucidate their functions experimentally [5]. Functional characterization of DNA elements benefits from a high-quality annotation of lncRNAs in genomes [6]. Integration of several orthogonal

transcriptomic data offers an opportunity to inform on the precise location of various lncRNA subtypes and alternative lncRNA isoforms from a single locus [6]. Experimental avenues to abolish specific lncRNA isoforms may trigger the generation of alternative isoforms that may partially substitute for functions, calling for a multi-facetted functional characterization of lncRNA loci [7, 8]. The resulting RNA molecules, but also the act of transcription generating lncRNA can regulate the expression of neighboring genes [9]. The act of transcription from an upstream lncRNA locus may trigger gene activation of the downstream, or gene repression, for instance by transcriptional interference [9]. Ribosome profiling (Ribo-seq) may suggest small open reading frames (sORFs) of the lncRNA loci [3]. Notably, lncRNA association with ribosomes may indicate either ribosome-coupled RNA degradation or translation [3]. Collectively, the broad range of candidate hypotheses by which lncRNA loci may play functional roles call for multiple approaches to distinguish alternative molecular mechanisms [10].

LncRNAs may regulate nearby genes in *cis* or distant genes in *trans* [11-13]. Compared to *cis*-acting lncRNAs, relatively fewer functions of *trans*-acting lncRNAs have been clarified [4]. A key experiment to distinguish between *cis*-acting and *trans*-acting mechanisms is to test phenotypic complementation of lncRNA loss-of-function mutants by lncRNA expression from a different genomic region [4]. *Trans*-acting lncRNAs regulate distant genes via different mechanisms [11], for example, through chromatin targeting of lncRNAs to fine tune chromatin architecture resulting in an altered transcriptional output [14]. Nevertheless, functional characterization of *trans*-acting lncRNAs remains a key knowledge gap to understand the regulatory contributions of the non-coding genome.

In plants, an increasing number of lncRNA loci have been implicated in the regulation of flowering time [15-20]. Flowering time represents a developmental transition of plants that is key for reproductive success. Genetic and environmental factors, for example, altered internal secondary metabolites (e.g. lignin), extended cold periods (i.e. vernalization) or day length (i.e. photoperiod), help plants to align flowering with favorable conditions [21-23]. Vernalization-induced flowering associates with several lncRNAs such as *COOLAIR*, *COLDAIR*, *ANTISENSE LONG* (*ASL*), and *COLDWRAP* that in *cis* repress gene expression of *FLOWERING LOCUS C* (*FLC*), a key flowering repressor at different stages of vernalization [24-27]. The contribution of *trans*-acting lncRNAs to the regulation of flowering time is currently unclear.

Here, we characterized the lncRNA locus *FLAIL* in *Arabidopsis* that gives rise to several RNA isoforms. Genomic mutations and strand-specific RNA repression provided evidence that *FLAIL* sense lncRNA repressed flowering. Genetic complementation data supported a *trans*-acting role of *FLAIL* in the regulation of flowering genes. *FLAIL* RNA bound the chromatin of flowering-related target genes that were differentially expressed in *flail* mutants, arguing for direct effects of *FLAIL* in flowering gene regulation. In summary, our data suggest flowering regulation through effects on gene expression by chromatin association of the *trans*-acting RNA *FLAIL*.

Results

Characterization of the *FLAIL* locus

FLAIL was annotated as a lncRNA in the TAIR [28] and GreeNC [29] databases and mapped as a single exon to chromosome 2 in *Arabidopsis* (Fig. 1A). Consistently, Nanopore RNA-seq data of chromatin-associated RNAs provided no evidence for splicing at the *FLAIL* locus [30] (Fig. S1A). Additionally, plaNET-seq used for genome-wide profiling of nascent RNA polymerase II (RNAPII) transcription [31], identified both sense and antisense isoforms at the *FLAIL* locus (Fig. 1A). We obtained additional information by examining RNA 5´-end mapping by TSS-seq [32] and simultaneous RNA 5´- and 3´-end mapping by TIF-seq [33] in the mutant of the nuclear exosome component *HUA ENHANCER2* (i.e. *hen2-2*). These data confirmed that the *FLAIL* locus was transcribed on both strands, since sense and antisense *FLAIL* transcripts were detected. Moreover, RNA isoforms derived from *FLAIL* were 5´-end capped, 3´-end polyadenylated and degraded by the nuclear exosome in *Arabidopsis* (Fig. 1A). To assess the protein-coding potential of *FLAIL* RNAs, we used the Coding Potential Calculator (CPC2) [34] and Coding-NonCoding Identifying Tool (CNIT) [35]. These analyses revealed poor coding potential of the lncRNA *FLAIL*, similar to other well-known ncRNAs (*18sRNA*, *U6*, *ELENA1*, *SVALKA*) [36, 37], but much lower than the protein coding potential of *UBIQUITIN* (*UBQ*) mRNA (Fig. 1B). Finally, an analysis of translation start sites in *FLAIL* RNAs suggested poor protein coding potential, well below the 0.5 threshold predicted for protein start codon as determined by the NetStart software package [38] (Fig. S2). Nevertheless, Ribo-seq [39, 40] data indicated ribosome association of *FLAIL* RNAs. This ribosome association could be consistent with translation of two sORFs with ~9 amino acids, or ribosome-mediated RNA degradation (Fig. S1B) [39]. In summary, the *FLAIL* locus harbors both sense and antisense lncRNA isoforms.

Even though lncRNAs show relatively poor sequence conservation [41], *trans*-acting lncRNAs may show signatures of conservation across species [42]. We identified a match in the genome of *Camelina sativa* on chromosome 17 (Fig. S3A). *Camelina*, like *Arabidopsis*, is in the Brassicaceae and last shared a common ancestor with *Arabidopsis* ~ 18 million years ago [43]. Reciprocal blast searches narrowed down a microhomology region between the sense *FLAIL* 3´-end in *Arabidopsis* and a non-coding DNA region near the *Camelina* gene *Csa17g011930.* In turn this region in *Camelina* is syntenic to a genomic region in *Arabidopsis* surrounding the *At1G08480* locus (Fig. S3A). Indeed, we successfully detected the existence of genomic *FLAIL-like* non-coding DNA by PCR amplification (Fig. S3C). We next performed RT-PCR targeting the *FLAIL-like* non-coding DNA region to examine RNA expression in *Camelina sativa* leaves and seedlings (Fig. S3B-C). Our data are consistent with the expression of RNA from the *FLAIL-like* non-coding DNA region in *Camelina sativa*, even though we detected noticeably weaker expression compared to *Arabidopsis FLAIL* expression in equivalent experimental conditions. In conclusion, our comparative genomic analysis identified a candidate *FLAIL-like* non-coding DNA region in Brassicaceaes with signatures of RNA expression.

***FLAIL* characterizes a *trans*-acting lncRNA repressing flowering**

To address the function of *FLAIL* in *Arabidopsis*, we used CRISPR/Cas9 technology with paired sgRNAs to generate two different *flail* knockout mutants with deletion fragments of 229 bp (*flail1*) [44], and 343 bp (*flail2*) (Fig. S4A-E). We also obtained a mutant line SAIL_645_C03 (*flail3)* carrying a T-DNA insertion at the 3´-end of sense *FLAIL* locus (Fig. S4A, F). All three mutants reduced the expression of sense and antisense *FLAIL* transcripts as detected by RT-qPCR, suggesting that they reduced the bioavailability of *FLAIL* isoforms (Fig. 1C-D). All three *flail* mutants flowered earlier than wild type (Fig. 1E-F). Our genetic data thus revealed a link between non-coding transcription at the *FLAIL* locus and flowering time.

To test which transcript of *FLAIL* was linked to the observed phenotype of the *flail* mutant we performed a complementation test. We transformed a DNA fragment encoding either sense or antisense *FLAIL* driven by the corresponding native promoter into the *flail3* mutant background with *GUS* driven by *35S* promoter as a control (Fig. 2A). Importantly, the constructs carried the *NOS* terminator that largely abolished initiation of antisense transcription [8, 37, 45]. We selected *flail3* for complementation because *FLAIL* disruption by T-DNA insertion at the 3´-end left potential sORF regions at the 5´-end intact (Fig. S4A). We selected two representative homozygous single locus insertion lines for each transformed construct (*flail3 pFLAIL:gFLAIL18/88* and *flail3 pasFLAIL:gasFLAIL18/39*) that expressed sense and antisense *FLAIL* at levels slightly higher than or similar to wild type (Fig. 2B-C). However, only exogenous expression of sense *FLAIL* rescued the early flowering phenotype of the *flail3* mutant (Fig. 2D-E), suggesting that the early flowering of the *flail* mutant was caused by the disruption of the sense *FLAIL* transcript isoform. In *Arabidopsis*, transgene insertion is non-targeted. We thus reasoned that complementation argued for the capability of sense *FLAIL* to act from a different genomic location, presumably as a *trans*-acting lncRNA. This hypothesis predicts that knock-down of sense *FLAIL* RNA should result in equivalent effects as genomic mutations. To test this hypothesis, we employed strand-specific RNA repression using artificial microRNAs (amiRNAs) [46]. We generated two amiRNA targets (*amiR-FLAIL-11* and *amiR-FLAIL-12*) (Additional file1: Fig. S5A), both exhibiting strongly reduced sense *FLAIL* transcription (Additional file1: Fig. S5B) and similar effects on flowering as genomic mutations (Additional file1: Fig. S5C-D). In conclusion, our experimental data indicate that the sense *FLAIL* lncRNA represses flowering through a *trans*-acting mechanism.

***FLAIL* lncRNA binding to chromatin regions promotes the expression of selected flowering repressors**

Early flowering in *Arabidopsis* may be associated with altered expression of flowering-related genes. To gain insight into the molecular basis of *FLAIL*-mediated regulation of flowering time, we determined

the transcriptional profiles of two-week old seedlings for wild type, *flail3,* and *flail3 pFLAIL:gFLAIL* with at least two independent replicates using stranded RNA-seq. Since the early flowering time effect in *flail3* could be rescued by *pFLAIL:gFLAIL*, we reasoned that this experimental setup may be suitable to identify gene expression changes directly correlated with sense *FLAIL* expression. Compared to wild type, 1221 differentially expressed genes (DEGs) were called by DESeq2 with at least two-fold change (adjusted *p* value < 0.05; Table S1), with 419 up-regulated and 802 down-regulated genes in *flail3* mutants. Almost half of these transcriptional differences in *flail3* reverted to wild-type expression level by exogenous expression of the *FLAIL* sense RNA into *flail3* mutants, including the *FLAIL* lncRNA itself (Fig. S6A and Fig. S7F, Table S2). We next focused on functional annotations of genes associated with the process of flowering [47]. Among the DEGs in *flail3*, we identified twenty genes linked to flowering (Fig. S6A). Expression of most of them were fully (eight) or partially (five) rescued by the expression of *pFLAIL:gFLAIL* (Fig. 3A-E, Fig. 4E-H, Fig. S6B, S7A-E and S9B, D). In conclusion, our transcriptomic data indicate potential targets for the *trans*-acting lncRNA *FLAIL*.

The reversible effect on flowering gene expression upon re-introduction of *pFLAIL:gFLAIL* argued for a direct effect of the *FLAIL* lncRNA. To identify where *FLAIL* bound chromatin regions, we performed chromatin isolation by RNA purification (ChIRP) of endogenous *FLAIL* followed by DNA-seq (*FLAIL* ChIRP-seq). We targeted sense *FLAIL* by two non-overlapping antisense oligonucleotide pools (Even and Odd probes, Fig. 4A bottom) tiled along the entire *FLAIL* transcript sequence compared to an oligonucleotide pool against the *LUCIFERASE* (*LUC*) mRNA as control that is not expressed in our strains. We efficiently captured the endogenous *FLAIL* RNA from chromatin compared to the unrelated *UBQ* mRNA (Fig. 4B). Moreover, *LUC*-specific probes did not enrich *FLAIL*, suggesting the specificity of RNA affinity purification in our assay conditions (Fig. 4B). After isolating DNA fragments associated with the *FLAIL*-containing complex, we assessed the genome-wide occupancy of *FLAIL* at high resolution by ChIRP-seq, followed by peak calling using CCAT3.0 [48]. Only peaks that occurred at target genes from both even and odd probe pools, but not from two or more independent experiments of Luc pools were considered significantly enriched (Fig. S8A). This analysis strategy allowed us to identify 210 target genes of *FLAIL* (Table S3). We observed a strong enrichment for the *FLAIL* locus by both ChIRP-seq (Fig. 4A, top) and ChIRP-qPCR (Fig. 4C). We noted that the *FLAIL* locus represented the only locus where we could expect binding, thus validating our identification strategy of genomic *FLAIL* binding. We analyzed the overlap between genes which were differentially expressed in the RNA-seq experiment and those genes that showed statistically significant *FLAIL* binding by ChIRP-seq (Fig. 4F). We identified twelve genes matching both criteria. At these targets, chromatin binding by *FLAIL* was linked to corresponding changes of gene expression, arguing for direct effects of *FLAIL* binding on gene expression. Four of these genes were functionally connected to flowering: *CIRCADIAN 1 (CIR1), LACCASE 8 (LAC8), PECTIN LYASE-LIKE 25 (PLL25) and PHOSPHOETHANOLAMINE N-METHYLTRANSFERASE 3 (NMT3)* (Table S4). All four flowering genes were transcriptionally down-regulated in *flail3* (Fig. 4D-E and 4G-H, Fig. S9A-D, Table S1).

However, the complementation construct failed to restore *NMT3* expression, arguing against a direct effect here (Fig. S9A-B, Table S2). A detailed examination revealed that *PLL25* regulates flower morphology rather than flowering time [49], arguing against effects on flowering time through mis-regulation of this gene [50, 51]. On the other hand, *cir1* [52] and *lac8* [53] mutants displayed early flowering phenotypes. These data suggest repression of *CIR1* and *LAC8* as candidate molecular hypothesis to explain the early flowering time phenotype in *flail* [52, 53]. In conclusion, our data suggest that *FLAIL* sense RNA represses flowering through inhibiting expression of the direct *FLAIL* targets *CIR1* and *LAC8*, consistent with a model where gene expression changes regulating flowering are mediated by interactions of the *trans*-acting lncRNA *FLAIL* with the genome (Fig. 4I).

Discussion

FLAIL functions in flowering time

In this study, we report repression of flowering time by the *trans*-acting lncRNA *FLAIL*. While many lncRNAs affect flowering regulation, the molecular mechanisms remain largely unclear [15-20]. Previously characterized lncRNAs including *COOLAIR*, *COLDAIR*, *ASL*, *COLDWRAP*, and *MAS* are transcribed from the flowering genes *FLC* or *MAF4* to locally affect their coding gene expression in *cis* [20, 24, 27, 54, 55]. We note that the *FLAIL* 3´-end resides approximately 130 bp upstream of the 5' UTR region of the *PORCUPINE* (*PCP*, also called *Sm protein E1*, *SME1*) gene, and *pcp/sme1* mutants flower early [56, 57]. We failed to find evidence for the hypothesis that *FLAIL* may affect flowering through *PCP* by a *cis*-acting mechanism. *FLAIL* neither regulates *PCP* expression nor shows overlapping effects on gene expression (Table S1 and S5-7, Fig. S10A-D).

In contrast, our work identifies a *trans*-acting *FLAIL* that represses flowering and binds multiple genomic loci. We thus favor the interpretation that *FLAIL* binding to other genomic regions explains the phenotypic effects of the mutants. For instance, *FLAIL* promotes the expression of the MYB family transcription factor *CIR1*, which in turn broadly contributes to gene expression. This may also explain why some genes are *FLAIL*-regulated but lack chromatin interactions with *FLAIL*. *CIR1* is a circadian clock gene, induced by light and involved in a regulatory feedback loop that controls a subset of the circadian outputs [52]. Our GO analysis supports that a subset of DEGs are connected to the response to red or far red light that contains among other key flowering genes such as *PHYTOCHROME INTERACTING FACTOR 4* (*PIF4*) and *CONSTANS* (*CO*) (Fig. S10B). *FLAIL* also binds the chromatin region of *LAC8*. LAC8 is a laccase family member that mainly modulates phenylpropanoid pathway for lignin biosynthesis [53, 58]. Similar to *flail*, *lac8* mutants flower early [53]. While intermediates in this pathway [59, 60] or dysregulation of lignin-related genes [21, 22, 61] could promote flowering in plants, the molecular connections of reduced *LAC8* expression to effects on flowering time will require further investigation. Nevertheless, our observations of reduced expression

of *LAC8* and *CIR1* in *flail*, combined with restored expression upon re-introduction of *FLAIL*, and direct *FLAIL* binding to *LAC8* and *CIR1* chromatin, suggested that early flowering in *flail* may result from combined direct and indirect effects of *LAC8* and *CIR1* repression.

The range of plausible candidate mechanisms by which *FLAIL* may promote gene expression includes targeting of chromatin modifying complexes to activate gene expression as shown for the mammalian lncRNA *HOTTIP* [62], or effects on pre-mRNA RNA processing to stimulate mRNA expression as indicated for the plant lncRNA *ASCO* [63-65]. While our results clarify key aspects of functional units of the non-coding genome, it will remain an exciting future research endeavor to elucidate how sense *FLAIL* mediates the activation of floral repressor genes at the molecular level.

Identification of the functional *FLAIL* RNA isoform of the *FLAIL* locus

A challenge in the field of lncRNA biology is the functional characterization of lncRNA loci. Our functional dissection of *FLAIL* illustrates these challenges, yet reveals a compelling example for a *trans*-acting lncRNA. Like many other loci, *FLAIL* generates multiple transcript isoforms, including cryptic transcript isoforms that would be missed by most standard transcriptomic approaches. DNA regulatory elements embedded in lncRNA loci and the act of lncRNA transcription may regulate the expression of neighboring genes (*cis*-acting) [66, 67]. However, disruption of the *FLAIL* locus had no significant impact on gene expression in a surrounding ~150 kb genomic window (from upstream AT2G18560 to downstream AT2G18940). These observations argue against the hypothesis that the *FLAIL* locus acts as a *cis*-acting RNA or DNA element. In contrast, we found genetic evidence that the *FLAIL* sense lncRNA functions as a *trans*-acting RNA. First, exogenous expression of *FLAIL* sense RNA *in vivo* rescues the early flowering phenotype as well as the expression of flowering genes in *flail3.* The rescue is specific for the *FLAIL* lncRNA encoded by the sense strand. Second, amiRNA mutants that specifically knock-down *FLAIL* sense RNA levels without effect on the DNA also show early flowering. Collectively, these data indicate that the role of the *FLAIL* locus in the repression of flowering is executed by a *trans*-acting lncRNA derived from the sense strand.

We assessed the protein-coding potential of *FLAIL* using a series of software tools that give low scores, arguing against a protein encoded by *FLAIL*. Nevertheless, Ribo-seq identifies ribosome association of *FLAIL,* consistent with two small ORFs with ~9 amino acids (Fig. S1B) [39]. Even though we found no evidence for peptide production in proteomics data, sORFs embedded in lncRNAs may encode for functional peptides [68, 69]. In our allelic series of *flail* mutants only *flail1* mutates the potential sORFs, while *flail2* and *flail3* keep the DNA sequences encoding the potential sORFs intact. The range of genetic mutations thus argue against the contribution of potential sORFs peptides to flowering, since the early flowering phenotype is similar in all three mutant backgrounds. Moreover, the microhomology with *Camelina* mapped to the 3'-region of *FLAIL* where we identified no ribosome association. While future experimental research in *Camelina sativa* would be needed to

examine functional conservation in flowering, the microhomology of *FLAIL* in other Brassicaceae is consistent with functional RNA domains that are a characteristic of conserved *trans*-acting lncRNAs.

Conclusions

In summary, this work highlights the contribution of lncRNAs to fine tune the complex developmental transition to initiate flowering. Regulation for key developmental decisions by lncRNA-based mechanisms may confer specific organismal advantages, yet detecting the functional roles of the non-coding genome may also be facilitated in the developmental context. RNA-based regulation of plant reproductive development through *trans*-acting lncRNA promises future possibilities for plant breeding research to improve Brassicaceae crop quality and resilience.

Methods

Plant materials and growth conditions

Table S8 provides a complete overview of the plant materials used in this study. Seeds of *flail3* (SMA2648, Table S8) were obtained from the Nottingham *Arabidopsis* Stock Centre and genotyping was performed using primers Mlo37/1788/1789 (Additional file 2 Table S9). *A. thaliana* plants were grown in a growth chamber with a long day photoperiod (16-h light/8-h dark) at 20 °C at a photo flux density of approximately 100 µmol/m^2/sec in the chamber. For seedling treatments, seeds were surface-sterilized and placed on ½ MS + 1% sucrose plates at 4 °C in darkness for 3 days prior to germination. Then, plates were placed in the growth chamber in control conditions at 20 °C and sampled.

CRISPR/Cas9-directed *flail* mutants

Construction of a dual sgRNA-directed *flail1* (*goi*, [44]) knockout SMA3677 (Table S8) was performed by CRISPR/Cas9 using the described protocol [44]. Similarly, to generate the CRISPR mutant *flail2* (SMA3678, Table S8), plasmid pHEE2E-TRI (SMC528) harboring two sets of gBlocks including gBlock1 (a U6-26 promoter, a 19 bp target sequence 1, a sgRNA scaffold, a terminator) and gBlock2 (a U6-29 promoter, a 19 bp target sequence 2, a sgRNA scaffold, a terminator) served as a template to amplify the middle border (BsaI-overhang1-protospacer1-scaffold-terminator-U6-29 promoter-protospacer2-overhang2-BsaI) using primer paris Mlo1757 & Mlo1758 (Table S9). Second, both pKIR1.1 plasmid (SMC529) and the middle border were digested by AarI and BsaI, respectively, then the middle border was integrated into the linearized pKIR1.1 backbone to generate pKIR1.1-dual-sgRNA2 SMC575 (Table S10) for plant transformation. Third, after transformation using *Agrobacterium tumefaciens* strain SMA111 (Table S11), the T1 generation plants for successful T-DNA insertion events were selected by identifying seeds with red fluorescence, then seeds from individual T1-genotyped plants were harvested and grown. Finally, T2 mutants that did not contain

the CRISPR/Cas9 construct were identified by picking up T2 seeds without red fluorescence. PCR products were amplified from Cas9-free T2 plants using oligonucleotides Mlo2478/2479 (Table S9) flanking the deletion site for Sanger sequencing.

Complementation assay

Complementation constructs were generated using SMC431. *pFLAIL:FLAIL* and *pasFLAIL:asFLAIL* were amplified from genomic wild type DNA using primers MLO1746/1747 and MLO1759/1761, respectively (Table S9). The resulting PCR products were inserted into pENTR-D-Topo by topo cloning to generate entry vectors SMC542 and SMC541 (Table S10). The entry vectors were used in a LR reaction with SMC431 to generate expression vector SMC546 (containing *pFLAIL:gFLAIL* construct) and SMC545 (containing *pasFLAIL:gasFLAIL* construct) (Table S10). The complementation constructs together with the control vector *35S:GUS* (SMC377) were then transformed into GV3101 to get strains SMA112-114 (Table S11), followed by transformation into the *flail3* mutant. Seeds from transformed *Arabidopsis* plants were screened for T-DNA integration by hygromycin resistance. Multiple independent single-locus insertions were identified by segregation analysis and homozygous T3 transgenic plants SMA4477 for *flail3 35S:GUS*, SMA4462 for *flail3 pFLAIL:gFLAIL18*, SMA4464 for *flail3 pFLAIL:gFLAIL88*, SMA4467 for *flail3 pasFLAIL:gasFLAIL18*, SMA4468 for *flail3 pasFLAIL:gasFLAIL39* were used for the complementation assay (Table S8).

Cloning of amiRNA

To construct *amiR-FLAILs*, we designed two artificial miRNA sequences in the miR319a backbone using Web MicroRNA Designer (WMD3) software to generate four oligonucleotide sequences (I to IV) (Mlo1774-1781, Table S9), which were used to engineer the amiRNA into the endogenous miR319a precursor by site-directed mutagenesis. The amiRNA containing precursor was generated by overlapping PCR using SMC532 as a template following the protocol described in the WMD3 publication [46]. The fragment containing the amiRNA sequence was then introduced into pENTR-D-Topo by topo cloning to generate entry vectors (SMC547 for *amiR-FLAIL11-Topo* and SMC548 for *amiR-FLAIL12-Topo*) (Table S10). The entry vectors were used in a LR reaction with SMC531 to generate expression vector SMC558 (containing *amiR-FLAIL11* construct) and SMC559 (containing *amiR-FLAIL12* construct). Plant transformation was performed using *Agrobacterium* strains SMA115-117 (Table S11). Finally, homozygous T3 transgenic plants SMA4469, SMA4471, and SMA4480 (Table S8) were used in this study.

Gene expression analysis by PCR/RT-(q)PCR

For the comparative expression analysis with *C. sativa*, genomic DNA was extracted from wild type *A. thaliana* and *C. sativa* seedlings (~1.5 weeks) and mature leaves (~4 weeks) using the DNeasy Plant Mini kit (Qiagen #69104) and diluted to 5 ng/µl. Total RNA was extracted from the same tissues

using the RNeasy Plant Mini kit (Qiagen #74904) with RNase-free DNase set (Qiagen #79254). Reverse transcription (RT) was performed on 1 µg of DNase-treated total RNA using the iScript cDNA synthesis kit (Bio-Rad #1708890), with the same amount of total RNA diluted in water as negative controls for RT-PCR. Primers (Table S9) were designed to amplify *AthaFLAIL* (*AT2G18735*), *CsatFLAIL-like* (*C. sativa*, Ensembl v51 Chr17 3432317-3432814), and *GAPDH* as an amplification control. Two reverse primers were designed to target different portions of *AthaFLAIL* and *CsatFLAIL-like*. The *GAPDH* primers amplify both *AthaGAPDH* and *CsatGAPDH*. PCR was performed with templates consisting of either 20 ng of genomic DNA, 50 ng of total RNA, or 50 ng of total RNA that had been reverse transcribed. 35 cycles of amplification were performed for all template types. PCR products were visualized after agarose gel electrophoresis using the Bio-Rad Chemi-doc imaging platform.

For reverse transcription quantitative real-time PCR, total RNA was extracted from two-week old *Arabidopsis* seedlings using an RNeasy Plant Mini Kit (Qiagen, Germany). DNA in the isolated RNA were digested with TURBO DNase (Thermo Fisher Scientific, USA). Purified RNA was subsequently reverse transcribed into cDNA with iScript™ cDNA Synthesis Kit (Bio-Rad, USA) following manufacturer's instructions. For real-time PCR analysis, the resulting cDNA was diluted ten-fold and used as a template in a PCR reaction with GoTaq qPCR Master mix (Promega, USA) and run on a CFX384 Touch instrument (Bio-Rad, USA) with an initial denaturation at 95 °C for 2 minutes, followed by 40 cycles at 95 °C for 15 seconds, 60 °C for 1 minute. Primer efficiencies were evaluated on a standard curve generated using a 10-fold dilution series of the sample over four dilution points. Relative expression was calculated and normalized to the internal reference gene *UBQ*. All primers (Table S9) did not show any evidence for non-specific products in the melting curve analysis.

Chromatin isolation by RNA purification (ChIRP)

ChIRP was performed as previously described with some modifications [70]. Probe design: The antisense oligonucleotide probes were designed against the full-length *FLAIL* sequence using the online probe designer at www.singlemoleculefish.com [71]. The probes were biotinylated at the 3′ end. To assess the specificity of the target capture by the oligonucleotides, the *FLAIL* probes were divided into two pools, Odd (Mlo2885) and Even (Mlo2886). All the experiments were carried out using both pools independently. Sixteen biotinylated oligonucleotide probes complementary to the *LUCIFERASE* transcript were pooled (Mlo2887) as negative control (Table S9).

RNA immunoprecipitation: Two-week old seedlings were crosslinked in 3% formaldehyde solution by vacuum infiltration for 25 minutes and then quenched by the addition of 0.125 M glycine at room temperature for 5 minutes. After washing and drying, crosslinked seedlings (2.5 g) were ground to a fine power in liquid nitrogen and suspended in 10 ml Honda Buffer (0.44 M Sucrose, 1.25% Ficoll, 2.5% Dextran T40, 20 mM Hepes KOH with pH 7.4, 10 mM $MgCl_2$, 0.5% Triton X-100, 5 mM DTT, 1

mM PMSF, 1 × Cocktail, and 2 U/ml RNase inhibitor). The samples were put on ice and mixed gently at 4 °C until the solution became homogenous, then filtered through two layers of Miracloth, centrifuged at 4000 rpm for 15 minutes at 4 °C. Pellets were resuspended in 1.5 ml Honda buffer and centrifuged at 4000 rpm for 15 minutes at 4 °C. Resuspending and centrifugation were repeated until the pellet was no longer green, typically two more times (~15 minutes). Pellets were suspended in 1600 µl nuclear lysis buffer (50 mM Tris-HCl, pH 7.5, 2 mM $MgCl_2$, 1% SDS, 0.1 mM PMSF, 10 mM EDTA, 1 mM DTT, 1 × Cocktail, 0.1 U/µl RNase Inhibitor) and sonicated at M setting 5 minutes (30 seconds on and 30 seconds off) × 3 times by sonicator (QSONICA Q700, USA) until DNA was fragmented into 200–500 bp pieces. After centrifugation at 12,000 g at 4 °C for 10 minutes, the supernatant (around 1.5 ml) was diluted with 2 volumes of pre-heated hybridization buffer (750 mM NaCl, 1% SDS, 50 mM Tris, pH 7.5, 1 mM EDTA, 15% formamide, and 1 × protease inhibitor). The clear mixture was divided into 4 equal aliquots (IP-RNA and IP-DNA for both Even and Odd probes). Biotinylated DNA probe (2 µl of 100 pmol/µl) was added to each aliquot and incubated at 37 °C for 4 hours with gentle mixing. Then 50 µl of well-washed Streptavidin C1 magnetic beads were added to each sample and incubated at 37 °C for 30 minutes. Captured beads were washed three times with high salt wash buffer (2 × SSC, 0.5% SDS, 1 mM DTT, and 1 mM PMSF) and three times with low salt wash buffer (0.1 × SSC, 0.5% SDS, 1 mM DTT. and 1 mM PMSF).

RNA isolation: Beads were resuspended in 200 µl RNA elution buffer (100 mM NaCl, 50 mM Tris-HCl with pH 7.5, 1 mM EDTA, 1% SDS) and boiled for 15 minutes. RNA samples were treated with Proteinase K (1 mg/ml) at 65 °C for 1 h while shaking. RNA was extracted using TRIzol method, and then treated with DNase (Qiagen). RNA was used for RT-qPCR analysis to confirm RNA retrieval.

DNA isolation: DNA was eluted with elution buffer (200 mM NaCl, 50 mM $NaHCO_3$, 1% SDS, 10% SDS, 0.1 U/µl RNase H). After Proteinase K treatment at 45 °C for 1 h, DNA was extracted using ChIP DNA Clean & Concentrator (Zymo Research) and used for subsequent qPCR analysis or high-throughput sequencing.

Comparative Genomics:

FLAIL sequence similarities were initially identified through reciprocal best BLAST against eleven disparate Brassicaceae genomes in CoGe BLAST [72] with an e-value of 10^{-5}. As no hits were identified in a species more distantly related than *Camelina sativa*, comparative analysis was restricted to *Arabidopsis* and *Camelina*. Genomic regions displaying sequence similarity to the *Arabidopsis FLAIL* locus in the *Arabidopsis thaliana* (TAIR10) and *Camelina sativa* (Ensembl v2.0) were identified using CoGe BLAST, with regions of microsynteny identified using GEvo [73]. Nucleotide sequence for syntenic regions were extracted and imported into Geneious Prime v2021.2.2 [74]. Multiple sequence alignments were used to design primers that specifically amplified a portion of *FLAIL* and the *FLAIL-like* intergenic region in *Camelina*.

Statistical analysis

The number of rosette leaves were measured with ImageJ software [75]). Statistical analysis was performed using the R software [76] or GraphPad Prism 9 [77]. For comparisons, data were evaluated using Student's t-test for significance of differences: * means p value < 0.05, ** means p value < 0.01.

Bioinformatics

All the supporting code for bioinformatics analysis is repository available at FLAIL_2021 from GitHub (https://github.com/Yu-Jin-KU) [78].

Sequencing analysis

RNA-seq libraries were prepared using NEXTFLEX® Rapid Directional RNA-seq Library Prep Kit (NOVA-5138-08) and ChIRP-seq libraries were constructed using the ChIP-seq Library Prep Kit (NOVA-5143-02 with NEXTflex® ChIP-seq Barcodes-24) following the manufacturer's protocol and quantified on Agilent 2100 Bioanalyzer. Both RNA-seq and ChIRP-seq libraries were pooled into one flow cell (NextSeq 500/550 High Output Kit v2.5) for sequencing in PE mode (2*75 bp) on Illumina Nextseq 500.

Previously published RNA-seq datasets for wild type and PCP (SME1) deficient plants were downloaded from European Nucleotide Archive (accession number PRJEB24412) and from Gene Expression Omnibus (accession number GSE116964). The raw reads were quality controlled by the FastQC software [79], adapter trimmed by Trimmomatic v0.39 [80] in paired-end mode and then aligned to TAIR10 genome assembly by STAR v2.7.8a [81] in Local mode. Aligned reads with MAPQ below 10 were removed by Samtools v1.1.2 [82]. BAM files were converted to unstranded Bedgraph files using BEDtools genomecov v2.30.0 [78]. The code was detailed in the RNA-seq.sh script on the GitHub page mentioned above. Differentially expressed genes (DEGs) were called using the DESeq2 tool [83]. Expression fold change values were log2 transformed to identify genes with statistically significant differential expression using the following criteria: |log2 fold change| > 1 and adjusted p value < 0.05. GO enrichment analysis was done by Metascape [47].

ChIRP-seq reads were quality controlled by the FastQC software [79], adapter trimmed using Trim Galore v0.6.7 [84] and mapped to the TAIR10 genome using STAR v2.7.8a [81]. The converted BAM files were sorted and filtered for MAPQ≥5. After removing PCR duplicates by Samtools v1.1.2 [82], peaks of *FLAIL* occupancy were called with CCAT3.0 [48]. By using CHIPseeker [85] and TxDb.Athaliana.BioMart.plantsmart28 [86] packages in R, peak annotation was performed with the definition for a promoter being 300 bp around the TSS. Alignment statistics were provided in Table S3. Visualization and analysis of genome-wide enrichment profiles were done with IGV genome browser [87].

Abbreviations

amiRNAs: artificial microRNAs

ChIRP: chromatin isolation by RNA purification;

CIR1: CIRCADIAN 1;

CNIT: Coding-NonCoding Identifying Tool;

CO: CONSTANS;

CPC2: Coding Potential Calculator;

DEGs: differentially expressed genes;

FLAIL: flowering associated intergenic lncRNA;

FLC: FLOWERING LOCUS C;

LAC8: LACCASE 8;

lncRNAs: long non-coding RNAs;

LUC: Luciferase;

NMT3: PHOSPHOETHANOLAMINE N-METHYLTRANSFERASE 3;

sORFs: small open reading frames;

PCP: PORCUPINE;

PIF4: PHYTOCHROME INTERACTING FACTOR 4

plaNET-seq: plant Native Elongating Transcripts sequencing

PLL25: PECTIN LYASE-LIKE 25;

RNAPII: RNA polymerase II;

SAMs: shoot apical meristems;

SME: Sm protein E1;

TIF-seq: Transcript Isoform sequencing;

TSS-seq: Transcription Start Site sequencing;

UBQ: UBIQUITIN

WMD: Web MicroRNA Designer

Figure legends

Fig. 1 Phenotypes of *FLAIL* knock-down plants. **A** Genome browser screenshot of plaNET-seq, TSS-seq and TIF-seq at the *FLAIL* genomic region in Col-0 and *hen2-2* mutant. Sense (+) and antisense (-) strands were shown in red and dark blue, respectively. Grey bar and light blue bar indicated primer locations of RT-qPCR for sense *FLAIL* (*FLAIL*) and antisense *FLAIL* (*asFLAIL*), respectively. **B** Coding potential of the transcript in the genomic region of *FLAIL* and *asFLAIL* and reference transcripts including non-coding RNAs (*18sRNA*, *U6*, *ELENA1*, *SVALKA*) and coding gene *UBQ* according to the CNIT and CPC2 algorithm. **C-D** Detection of *FLAIL* and *asFLAIL* gene expression in

Col-0 and *flail* mutants by RT-qPCR. Transcript levels were normalized to *UBQ* expression levels. Y-axis showed relative values compared to the expression level of Col-0. Bars represented average ± s.e.m (n = 3 independent 14-d seedling pools). *, *p* value < 0.05 and **, *p* value < 0.01 by Student's t-test compared to Col-0. **E** Morphological phenotypes of 4-week-old plants of Col-0, *flail* mutants at 20 °C under a 16-h light/8-h dark growth condition. Scale bar: 2 cm. **F** Violin graph showed number of rosette leaves after appearance of the first flower bud in Col-0. Data represented the mean of six independent experiments. Boxes spanned the first to third quartile, bold black lines indicated median value for each group and whiskers represented the minimum and maximum values. *, *p* value < 0.05 was indicated by Student's t-test compared to Col-0.

Fig. 2 *Sense-FLAIL* RNA is functional for flowering. **A** Schematic representations of the T-DNA constructs containing the native promoter of *sense-FLAIL* (native-Pro) fused to the *sense-FLAIL* DNA region with NOS as a terminator or the native promoter of *anti-sense FLAIL* (anti-native-Pro) fused to the *anti-sense FLAIL* DNA region or a negative control with the 35S promoter (35S) fused to GUS reporter were transformed into *flail3 Arabidopsis* plants. **B-C** Detection of *FLAIL* and *asFLAIL* genes expression in Col-0, *flail3* mutant and complemented lines expressing *pFLAIL:gFLAIL* and *pasFLAIL:gasFLAIL* by RT-qPCR. Transcript levels were normalized to *UBQ* expression levels. Y-axis showed relative values compared to the expression level of Col-0. Error bars represented s.e.m (n = 3 independent 14-d seedling pools). *, *p* value < 0.05 and **, *p* value < 0.01 by Student's t-test compared to Col-0. **D** Representative morphological phenotypes of 4-week-old plants of Col-0, *flail3* mutant, transgenic lines at 20 °C under a 16-h light/8-h dark growth condition. Scale bar: 2 cm. **E** Violin graph showed number of rosette leaves after appearance of the first flower bud in Col-0. Data represented the mean of six independent experiments. Boxes spanned the first to third quartile, bold black lines indicated median value for each group and whiskers represented the minimum and maximum values. *, *p* value < 0.05 was indicated by Student's t-test compared to Col-0.

Fig. 3 *FLAIL* regulates flowering related genes. **A** Heatmap and hierarchical clustering of top 70 differentially expressed genes (DEGs) in *flail3 versus* Col-0 that were best rescued in the *flail3 pFLAIL:gFLAIL18* complementation line. DEGs analyzed by DESeq2 with |log2 fold change| > 1 and adjusted *p* value < 0.05 were considered significant differential expression. Three biological replicates for *flail3*, wild type, and two for *flail3 pFLAIL:gFLAIL18.* Flowering genes were highlighted in yellow bold. Samples clustered together on the basis of corresponding similar expression profiles. The color scale reflected the log 2-fold change in gene expression, ranging from down-regulated (blue) to up-regulated (red). **B-E** Genome browser screenshots illustrating the expression of dysregulated flowering genes in *flail3* were rescued in complementation line (top panel). Normalized read counts (TPM from RNA-seq) for differentially expressed flowering genes in WT, *flail3*, and *flail3 pFLAIL:gFLAIL18* plants (bottom panel). Boxes spanned the first to third quartile, bold black lines

indicated median value for each group and whiskers represented the minimum and maximum values. All *p* values were denoted by Students' t-test. Bar = 500 bp.

Fig. 4 *FLAIL* affects flowering by chromatin binding of flowering genes. **A** Top, *FLAIL* bound the locus itself by ChIRP-seq from two independent Odd and Even probed chromatins. Luc probe was used as a control. Bottom, schematic representation of the antisense oligonucleotide probes that were biotinylated at the 3′-end with Odd (in red) and Even (in dark blue) against *FLAIL* sense RNA and Luc probe (in grey) against *LUC* mRNA. **B** ChIRP-qPCR using probe pools *FLAIL*-asDNA (Odd and Even) retrieved ~5%–10% of *FLAIL* endogenous RNA and < 1% levels of *UBQ*. *Luc*-asDNA probes retrieved much lower levels of both RNAs as a control. **C** *FLAIL* DNA signal was identified in both Odd and Even probes. *UBQ* region showed much less binding signal in all probes as a negative control. Graphs in **B** & **C** showed the mean ± s.e.m. (n= 3 independent replicates). **D, G** Genome browser screenshots illustrating two of *FLAIL* bound targets *CIR1* (**D**) and *LAC8* (**G**) in RNA-seq (lane 1-3) and ChIRP-seq (lane 4-6). FLAIL binding peaks were called by CCAT3.0 with the cutoff FDR = 0.232. **E, H** Normalized read counts (TPM from RNA-seq) for differentially expressed (DE) flowering genes in WT, *flail3*, and *flail3 pFLAIL:gFLAIL18* plants (bottom panel). Boxes spanned the first to third quartile, bold black lines indicated median value for each group and whiskers represented the minimum and maximum values. **F** Venn diagram of genes targeted by *FLAIL* (ChIRP-seq) and genes overlapped with DEGs in *flail3* and flowering related genes. **I** A model for the *trans*-acting *FLAIL* sense RNA regulated flowering. The *FLAIL* sense RNA binds chromatin regions of flowering genes to regulate expression levels of flowering related genes and thus affects flowering time. All *p* values were denoted by Students' t-test.

Supplementary information

Fig. S1 Characterization of *FLAIL* locus. **A** Genome browser view of *FLAIL* splicing status in nanopore sequencing of Col-0. Transcription of sense *FLAIL* RNA and *asFLAIL* RNA were shown in red and dark blue, respectively and no isoform resulting from alternative splicing was observed. **B** *FLAIL* nucleotide sequences in black and two sORFs locations in blue.

Fig. S2 Assessment of *FLAIL* and *UBQ* for protein coding potential. Initiation codon translational analysis using NetStart for *FLAIL* and *UBQ*. The predicted initiation codons were depicted with the letter i, other instances of "ATG" by the letter "N" (non-start). The dots (".") were place holders for all the other sequence elements. The scores were always in [0.0, 1.0]; when greater than 0.5, they represented a probable translation start.

Fig. S3 Sequence and transcriptional conservation at the *FLAIL* and *FLAIL-like* loci in *Arabidopsis* and *Camelina*. **A** Schematic depicting the conservation of the *Arabidopsis* (*A.tha*) *FLAIL* locus in *Camelina sativa* (*C.sat*). Green boxes represent exons, with triangles representing direction of transcription. The *FLAIL* locus is represented by a yellow box. Faded blue lines represent sequence similarity between different loci. Dashed boxes at the *FLAIL* and *Csa17g011930* loci represent regions targeted for RT-PCR. **B** Amplification of *A.thaFLAIL* and *C.satFLAIL*-like, using RNA template (+/- RT, lanes 1-20). NT indicates no template was added to the reaction. **C** Control amplifications: *GAPDH* was amplified using RNA template (+/- RT, lanes 21-29), and *A.thaFLAIL* and *C.satFLAIL-like* were amplified using genomic DNA template (lanes 30-41). L indicates leaf tissue, S indicates seedling tissue.

Fig. S4 *FLAIL* dual-sgRNA approach and T-DNA insertion genotyping. **A** Schematic representation of targeted gene *FLAIL* with locations of two Cas9-directed mutants *flail1*, *flail2*, and one T-DNA mutant *flail3*. Locations of dual-sgRNA target sites were shown in red arrow, primer pair F/R (Mlo2478/2479) were used for PCR testing deletion in *flail1* and *flail2*, triangle indicated the putative position of T-DNA insertion at the *FLAIL* locus. Blue boxes indicated two sORFs. **B** Similar to the previous generation of *flail1*, *FLAIL2* construct containing pKIR1.1 enabled red fluorescence selection of *flail2* seeds from T1 plants after transformation by floral dipping. **C** Genotyping of individual T1 plant with red fluorescence, Leaf genomic DNA of T1 plants were PCR amplified. Expected size of PCR product for deletion was 343 bp in *flail2* line. *flail2-32* in red box was selected for next generation. **D** In T2 selection, the null mutant *flail2-32-93* without red fluorescence in seeds represented Cas9-free plants, indicated by red box in **E**. PAM was shown in blue, sgRNA protospacers were in red, and deleted bases were replaced by dots. **E** PCR analysis of T2 lines. The expected size of the wild-type *FLAIL* amplicon and the deletion size between Cas9 cut sites in *flail2-32-93* were indicated. This inherited Cas9-null segregation line was used for data analysis in Fig. 1. **F** Genotyping of the T-DNA insertion mutant *flail3*. Gel sample order (from left to right): lane 1, marker; lane 2, WT; lane 3, *flail3*, with primer set, Mlo1788 + Mlo1789 + Mlo37; Results clearly showed that *flail3* line was homozygous since WT was the only line giving WT band and *flail3* line gave the only T-DNA insertion band.

Fig. S5 *FLAIL* lncRNA functions as a flowering repressor. **A** Sequences and structures of amiRNA duplexes and the target sites of *amiR-FLAILs* and *amiR-FLAIL*s*. Upper panel, schematic representation of transcribed sense *FLAIL* RNA. Lower panel, sequences of amiRNA duplexes, amiRNA (in red) target sites, and potential amiRNA* (in blue) on cognate sense *FLAIL* (in black). **B** Gene expression of *sense FLAIL* in *amiR-FLAIL* plants by RT-qPCR. Transcript levels were normalized to *UBQ* expression levels. Two representative lines for amiRNA designed transgenic plants were selected. Y-axis showed relative values compared to the expression level of empty vector transformed plants. Grey bars depicted the relative positions of primers used for RT-qPCR analyses.

583 Transcript levels were normalized to *UBQ* expression levels. Error bars represented s.e.m (n = 3
584 independent 14-day seedling pools). **, *p* value < 0.01 analyzed by Student's t-test. **C** Morphological
585 phenotypes of 4-week-old plants of Col-0 and two *amiR-FLAIL* plants under a 16-h light/8-h dark
586 growth condition. Scale bar: 2 cm. **D** Violin graph showed number of rosette leaves after appearance
587 of the first flower bud in Col-0. Data represented the mean of six independent experiments. Boxes
588 spanned the first to third quartile, bold black lines indicated median value for each group and whiskers
589 represented the minimum and maximum values. **, *p* value < 0.01 was indicated by Student's t-test
590 compared to Col-0.
591
592 **Fig. S6** Genome-wide effects of *FLAIL* on gene expression by RNA-seq. **A** Venn diagram of flowering
593 genes overlapped with upregulated and downregulated genes in the *flail3* mutant and with unchanged
594 genes in the *flail3 pFLAIL:gFLAIL18* complementation plant. **B** Reproducibility of all genes shown in
595 Fig. 3 from RNA-seq data was demonstrated by clustered heatmap of Pearson correlation coefficients
596 over all independent replicates of RNA-seq in WT, *flail3* mutant, and *flail3 pFLAIL gFLAIL18* plants.
597 Darker red denoted higher correlation and darker blue represented low reproducibility.
598
599 **Fig. S7** *FLAIL* regulates flowering related genes in *trans.* **A-F** Genome browser screenshots
600 illustrating the expression of dysregulated flowering genes in *flail3* were most fully rescued in
601 complementation line. Normalized read counts (TPM from RNA-seq) were used for differentially
602 expressed flowering genes in WT, *flail3*, and *flail3 pFLAIL:gFLAIL18* plants. Boxes spanned the first
603 to third quartile, bold black lines indicated median value for each group and whiskers represented the
604 minimum and maximum values. *p* value was denoted by Students' t-test.
605
606 **Fig. S8** Strategy to identify genome-wide binding profile of *FLAIL* analyzed by ChIRP-seq. **A**
607 Illustration of *FLAIL* peaks called by CCAT3.0. Only peaks that occurred at target genes from both
608 Even and Odd probed DNA, but not from two or more independent experiments of Luc pools were
609 considered significant enrichment (Example 1), peaks that only occurred from either Even or Odd
610 pools were not considered *FLAIL* targets (Example 2 & 3). **B** A pie chart that was generated by
611 ChIPseeker represented distribution of *FLAIL* bound regions in the genome. A total of 210 *FLAIL*
612 bound regions were annotated according to the genomic distribution and *FLAIL* was enriched
613 predominantly in promoter regions.
614
615 **Fig. S9** *FLAIL* binds chromatin regions of flowering genes for gene regulation. **A, C** Genome browser
616 screenshots illustrating two more *FLAIL* bound flowering targets *PLL25* and *NMT3* in RNA-seq (lane
617 1-3) and ChIRP-seq (lane 4-6). Their expression that was downregulated in *flail3* (lane 1) can be
618 partially or fully rescued in complementation line (lane 2). Both Odd and Even probes identified
619 chromatin binding regions of *FLAIL* in two more flowering genes *NMT3* and *PLL25* compared to *Luc*

620 probes. *FLAIL* binding peaks were called by CCAT3.0. **B, D** Normalized read counts (TPM from RNA-
621 seq) for differentially expressed (DE) flowering genes in WT, *flail3*, and *flail3 pFLAIL:gFLAIL18* plants
622 (bottom panel). Boxes spanned the first to third quartile, bold black lines indicated median value for
623 each group and whiskers represented the minimum and maximum values. *p* value was denoted by
624 Students' t-test.
625
626 **Fig. S10** *FLAIL* regulates flowering independent of *PCP.* **A, B** Venn diagram showing overlapping
627 differentially expressed genes (up/down) sets between *flail3* and *pcp* (also called *sme1*) mutants. **C,**
628 **D** GO analysis of the DEGs in RNA-seq data of *flail3* and *pcp /sme1* mutants. Y-axis indicated the
629 GO categories including biological process (BP), cellular component (CC) and molecular function
630 (MF); X-axis showed -Log10 *p* value with the cutoff 0.05. Highly enriched GO terms of dysregulated
631 mRNAs analyzed by the Metascape with 5 top enrichment scores.
632
633 **Table S1.** DEGs in *flail3* mutant
634 **Table S2.** DEGs in *flail3 pFLAIL gFLAIL18* plants
635 **Table S3.** *FLAIL* targets called by CCAT3.0
636 **Table S4.** Overlapping genes between DEGs in *flail3* and *FLAIL* targets.
637 **Table S5.** Gene Ontology of DEGs in *flail3*
638 **Table S6.** Gene Ontology of DEGs in *pcp* (RNA-seq data from Capovilla et al with the ENA accession:
639 PRJEB24412)
640 **Table S7.** Gene Ontology of DEGs in *sme1* (RNA-seq data from Huertas et al with the GEO accession:
641 GSE116964)
642 **Table S8.** Seeds
643 **Table S9.** Primer sequences
644 **Table S10.** Plasmids
645 **Table S11.** GV3101 strains
646

647 Declarations

648

649 Ethics approval and consent to participate

650 Not applicable
651

652 Consent for publication

653 Not applicable
654

655 Availability of data and materials

The RNA-seq and ChIRP-seq data were deposited at GEO with the number GSE186215 [88]. The reagents described in this study are available from the corresponding author.

Competing interests

The authors declare they have no competing interests.

Funding

S.M. acknowledges the funding from the Novo Nordisk Foundation (NNF15OC0014202, NNF19OC0057485), a Copenhagen Plant Science Centre Young Investigator Starting grant and EMBO YIP. This project receives support from the European Research Council (ERC) under the European Union's Horizon 2020 Research and Innovation Programme (StG2017-757411 to S.M.). A.D.L.N. would like to acknowledge funding from NSF-IOS 1758532 and NSF-IOS 2023310.

Authors' contributions

Y.J. and S.M. conceived the study. Y.J. performed most experimental work, A.N.D. and A.D.L.N contributed comparative genomics and expression analysis in S3. M.I. and Y.J. did the computational analysis. Y.J. and M.S. wrote the manuscript.

Acknowledgements

We thank Prof. Anders H. Lund and for kindly providing Luc probes. We thank Prof. Peter Brodersen for sharing amiRNA vectors. We thank Dr. Pan Zhu and Dr. Marta Montes for assistance with ChIRP, Prof. Egle Kudirkiene and Dr. Quentin Thomas for sequencing. We thank Jasmin Dilgen, Evangelia Lakita, Ida Damholt Richardt, Lei Li for technical assistance, Jan Høstrup for excellent plant care, Dr. Deyong Zhu and the members of Marquardt lab for discussions and manuscript feedback.

References

1. Osman S, Cramer P. Structural Biology of RNA Polymerase II Transcription: 20 Years On. Annu Rev Cell Dev Bi. 2020;36:1-34.
2. Kapranov P, Cheng J, Dike S, Nix DA, Duttagupta R, Willingham AT, Stadler PF, Hertel J, Hackermuller J, Hofacker IL, et al. RNA maps reveal new RNA classes and a possible function for pervasive transcription. Science. 2007;316:1484-1488.
3. Choi SW, Kim HW, Nam JW. The small peptide world in long noncoding RNAs. Brief Bioinform. 2019;20:1853-1864.
4. Gil N, Ulitsky I. Regulation of gene expression by cis-acting long non-coding RNAs. Nature Reviews Genetics. 2020;21:102-117.
5. Goff LA, Rinn JL. Linking RNA biology to lncRNAs. Genome Res. 2015;25:1456-1465.
6. Ivanov M, Sandelin A, Marquardt S. TrancriptomeReconstructoR: data-driven annotation of complex transcriptomes. Bmc Bioinformatics. 2021;22:290.
7. Jin Y, Marquardt S. Winter fields antisense RNAs to kick off flowering. Gene Dev. 2021;35:785-786.
8. Zhao YS, Zhu P, Hepworth J, Bloomer R, Antoniou-Kourounioti RL, Doughty J, Heckmann A, Xu CY, Yang HC, Dean C. Natural temperature fluctuations promote COOLAIR regulation of FLC. Gene Dev. 2021;35:888-898.
9. Gowthaman U, Garcia-Pichardo D, Jin Y, Schwarz I, Marquardt S. DNA Processing in the Context of Noncoding Transcription. Trends Biochem Sci. 2020;45:1009-1021.
10. Chen L, Zhu QH, Kaufmann K. Long non-coding RNAs in plants: emerging modulators of gene activity in development and stress responses. Planta. 2020;252:92.
11. Kopp F, Mendell JT. Functional Classification and Experimental Dissection of Long Noncoding RNAs. Cell. 2018;172:393-407.
12. Ariel F, Lucero L, Christ A, Mammarella MF, Jegu T, Veluchamy A, Mariappan K, Latrasse D, Blein T, Liu C, et al. R-Loop Mediated trans Action of the APOLO Long Noncoding RNA. Mol Cell. 2020;77:1055-1065.
13. Moison M, Pacheco JM, Lucero L, Fonouni-Farde C, Rodriguez-Melo J, Mansilla N, Christ A, Bazin J, Benhamed M, Ibanez F, et al. The lncRNA APOLO interacts with the transcription factor WRKY42 to trigger root hair cell expansion in response to cold. Mol Plant. 2021;14:937-948.
14. Mishra K, Kanduri C. Understanding Long Noncoding RNA and Chromatin Interactions: What We Know So Far. Noncoding RNA. 2019;5:54.
15. Fan YR, Yang JY, Mathioni SM, Yu JS, Shen JQ, Yang XF, Wang L, Zhang QH, Cai ZX, Xu CG, et al. PMS1T, producing phased small-interfering RNAs, regulates photoperiod-sensitive male sterility in rice. P Natl Acad Sci USA. 2016;113:15144-15149.

16. Ding JH, Lu Q, Ouyang YD, Mao HL, Zhang PB, Yao JL, Xu CG, Li XH, Xiao JH, Zhang QF. A long noncoding RNA regulates photoperiod-sensitive male sterility, an essential component of hybrid rice. P Natl Acad Sci USA. 2012;109:2654-2659.
17. Fang J, Zhang FT, Wang HR, Wang W, Zhao F, Li ZJ, Sun CH, Chen FM, Xu F, Chang SQ, et al. Ef-cd locus shortens rice maturity duration without yield penalty. P Natl Acad Sci USA. 2019;116:18717-18722.
18. Henriques R, Wang H, Liu J, Boix M, Huang LF, Chua NH. The antiphasic regulatory module comprising CDF5 and its antisense RNA FLORE links the circadian clock to photoperiodic flowering. New Phytol. 2017;216:854-867.
19. Severing E, Faino L, Jamge S, Busscher M, Kuijer-Zhang Y, Bellinazzo F, Busscher-Lange J, Fernandez V, Angenent GC, Immink RGH, Pajoro A. Arabidopsis thaliana ambient temperature responsive lncRNAs. Bmc Plant Biol. 2018;18:145.
20. Zhao XY, Li JR, Lian B, Gu HQ, Li Y, Qi YJ. Global identification of Arabidopsis lncRNAs reveals the regulation of MAF4 by a natural antisense RNA. Nat Commun. 2018;9.
21. Shi Y, Zhang X, Xu ZY, Li L, Zhang C, Schlappi M, Xu ZQ. Influence of EARLI1-like genes on flowering time and lignin synthesis of Arabidopsis thaliana. Plant Biology. 2011;13:731-739.
22. Xu B, Sathitsuksanoh N, Tang YH, Udvardi MK, Zhang JY, Shen ZX, Balota M, Harich K, Zhang PYH, Zhao BY. Overexpression of AtLOV1 in Switchgrass Alters Plant Architecture, Lignin Content, and Flowering Time. Plos One. 2012;7: e47399.
23. Cho LH, Yoon J, An G. The control of flowering time by environmental factors. Plant Journal. 2017;90:708-719.
24. Csorba T, Questa JI, Sun QW, Dean C. Antisense COOLAIR mediates the coordinated switching of chromatin states at FLC during vernalization. P Natl Acad Sci USA. 2014;111:16160-16165.
25. Liu FQ, Marquardt S, Lister C, Swiezewski S, Dean C. Targeted 3 ' Processing of Antisense Transcripts Triggers Arabidopsis FLC Chromatin Silencing. Science. 2010;327:94-97.
26. Swiezewski S, Liu FQ, Magusin A, Dean C. Cold-induced silencing by long antisense transcripts of an Arabidopsis Polycomb target. Nature. 2009;462:799-U122.
27. Shin JH, Chekanova JA. Arabidopsis RRP6L1 and RRP6L2 Function in FLOWERING LOCUS C Silencing via Regulation of Antisense RNA Synthesis. PLoS genetics. 2014;10:e1004612.
28. Poole RL. The TAIR database. Methods Mol Biol. 2007;406:179-212.
29. Gallart AP, Pulido AH, de Lagran IAM, Sanseverino W, Cigliano RA. GREENC: a Wiki-based database of plant lncRNAs. Nucleic Acids Res. 2016;44:D1161-D1166.
30. Jia JB, Long YP, Zhang H, Li ZW, Liu ZJ, Zhao Y, Lu DD, Jin XH, Deng X, Xia R, et al. Post-transcriptional splicing of nascent RNA contributes to widespread intron retention in plants. Nat Plants. 2020;6:780-788.

749 31. Kindgren P, Ivanov M, Marquardt S. Native elongation transcript sequencing reveals temperature
750 dependent dynamics of nascent RNAPII transcription in Arabidopsis. Nucleic Acids Res. 2020;48:2332-
751 2347.
752 32. Nielsen M, Ard R, Leng X, Ivanov M, Kindgren P, Pelechano V, Marquardt S. Transcription-driven
753 chromatin repression of Intragenic transcription start sites. PLoS genetics. 2019;15:e1007969.
754 33. Thomas QA, Ard R, Liu JH, Li BN, Wang JW, Pelechano V, Marquardt S. Transcript isoform sequencing
755 reveals widespread promoter-proximal transcriptional termination in Arabidopsis. Nat Commun.
756 2020;11:2589.
757 34. Kang YJ, Yang DC, Kong L, Hou M, Meng YQ, Wei LP, Gao G. CPC2: a fast and accurate coding potential
758 calculator based on sequence intrinsic features. Nucleic Acids Res. 2017;45:W12-W16.
759 35. Guo JC, Fang SS, Wu Y, Zhang JH, Chen Y, Liu J, Wu B, Wu JR, Li EM, Xu LY, et al. CNIT: a fast and
760 accurate web tool for identifying protein-coding and long non-coding transcripts based on intrinsic
761 sequence composition. Nucleic Acids Res. 2019;47:W516-W522.
762 36. Seo JS, Sun HX, Park BS, Huang CH, Yeh SD, Jung C, Chua NH. ELF18-INDUCED LONG-NONCODING RNA
763 Associates with Mediator to Enhance Expression of Innate Immune Response Genes in Arabidopsis.
764 Plant Cell. 2017;29:1024-1038.
765 37. Kindgren P, Ard R, Ivanov M, Marquardt S. Transcriptional read-through of the long non-coding RNA
766 SVALKA governs plant cold acclimation. Nat Commun. 2018;9:4561.
767 38. Pedersen AG, Nielsen H. Neural network prediction of translation initiation sites in eukaryotes:
768 Perspectives for EST and genome analysis. Fifth International Conference on Intelligent Systems for
769 Molecular Biology, Proceedings. 1997:226-233.
770 39. Palos K, Dittrich AN, Yu LA, Brock JR, Wu L, Sokolowska E, Skirycz A, Hsu PD, Lyons E, Beilstein MA,
771 Nelson ADL. Identification and Functional Annotation of Long Intergenic Non-coding RNAs in the
772 Brassicaceae. bioRxiv. 2021; doi:10.1101/2021.09.17.460835.
773 40. Hsu PY, Calviello L, Wu HYL, Li FW, Rothfels CJ, Ohler U, Benfey PN. Super-resolution ribosome profiling
774 reveals unannotated translation events in Arabidopsis. P Natl Acad Sci USA. 2016;113:E7126-E7135.
775 41. Nelson ADL, Forsythe ES, Devisetty UK, Clausen DS, Haug-Batzell AK, Meldrum AMR, Frank MR, Lyons
776 E, Beilstein MA. A Genomic Analysis of Factors Driving lincRNA Diversification: Lessons from Plants.
777 G3-Genes Genom Genet. 2016;6:2881-2891.
778 42. Ross CJ, Rom A, Spinrad A, Gelbard-Solodkin D, Degani N, Ulitsky I. Uncovering deeply conserved motif
779 combinations in rapidly evolving noncoding sequences. Genome biology. 2021;22.
780 43. Beilstein MA, Nagalingum NS, Clements MD, Manchester SR, Mathews S. Dated molecular phylogenies
781 indicate a Miocene origin for Arabidopsis thaliana. P Natl Acad Sci USA. 2010;107:18724-18728.

44. Jin Y, Marquardt S. Dual sgRNA-based Targeted Deletion of Large Genomic Regions and Isolation of Heritable Cas9-free Mutants in Arabidopsis. Bio-Protocol. 2020;10:e3796.
45. Fedak H, Palusinska M, Krzyczmonik K, Brzezniak L, Yatusevich R, Pietras Z, Kaczanowski S, Swiezewski S. Control of seed dormancy in Arabidopsis by a cis-acting noncoding antisense transcript. P Natl Acad Sci USA. 2016;113:E7846-E7855.
46. Schwab R, Ossowski S, Riester M, Warthmann N, Weigel D. Highly specific gene silencing by artificial microRNAs in Arabidopsis. Plant Cell. 2006;18:1121-1133.
47. Zhou YY, Zhou B, Pache L, Chang M, Khodabakhshi AH, Tanaseichuk O, Benner C, Chanda SK. Metascape provides a biologist-oriented resource for the analysis of systems-level datasets. Nat Commun. 2019;10:1523.
48. Xu H, Handoko L, Wei XL, Ye CP, Sheng JP, Wei CL, Lin F, Sung WK. A signal-noise model for significance analysis of ChIP-seq with negative control. Bioinformatics. 2010;26:1199-1204.
49. Chen W, Salari H, Taylor MC, Jost R, Berkowitz O, Barrow R, Qiu D, Branco R, Masle J. NMT1 and NMT3 N-Methyltransferase Activity Is Critical to Lipid Homeostasis, Morphogenesis, and Reproduction. Plant physiology. 2018;177:1605-1628.
50. Lashbrook CC, Cai S. Cell wall remodeling in Arabidopsis stamen abscission zones: Temporal aspects of control inferred from transcriptional profiling. Plant signaling & behavior. 2008;3:733-736.
51. Sun LX, van Nocker S. Analysis of promoter activity of members of the PECTATE LYASE-LIKE (PLL) gene family in cell separation in Arabidopsis. Bmc Plant Biol. 2010;10:152.
52. Zhang X, Chen Y, Wang ZY, Chen Z, Gu H, Qu LJ. Constitutive expression of CIR1 (RVE2) affects several circadian-regulated processes and seed germination in Arabidopsis. The Plant journal : for cell and molecular biology. 2007;51:512-525.
53. Cai XN, Davis EJ, Ballif J, Liang MX, Bushman E, Haroldsen V, Torabinejad J, Wu YJ. Mutant identification and characterization of the laccase gene family in Arabidopsis. J Exp Bot. 2006;57:2563-2569.
54. Heo JB, Sung S. Vernalization-Mediated Epigenetic Silencing by a Long Intronic Noncoding RNA. Science. 2011;331:76-79.
55. Kim DH, Sung S. Vernalization-Triggered Intragenic Chromatin Loop Formation by Long Noncoding RNAs. Dev Cell. 2017;40:302-312.
56. Capovilla G, Delhomme N, Collani S, Shutava I, Bezrukov I, Symeonidi E, Amorim MD, Laubinger S, Schmid M. PORCUPINE regulates development in response to temperature through alternative splicing. Nat Plants. 2018;4:534-539.
57. Huertas R, Catala R, Jimenez-Gomez JM, Castellano MM, Crevillen P, Pineiro M, Jarillo JA, Salinas J. Arabidopsis SME1 Regulates Plant Development and Response to Abiotic Stress by Determining Spliceosome Activity Specificity. Plant Cell. 2019;31:537-554.

816 58. Wang CY, Zhang SC, Yu Y, Luo YC, Liu Q, Ju CL, Zhang YC, Qu LH, Lucas WJ, Wang XJ, Chen YQ. MiR397b
817 regulates both lignin content and seed number in Arabidopsis via modulating a laccase involved in
818 lignin biosynthesis. Plant Biotechnol J. 2014;12:1132-1142.
819 59. Nakanishi F, Kusumi T, Inoue Y, Fujii T. Dihydrokaempferol Glucoside from Cotyledons Promotes
820 Flowering in Pharbitis-Nil. Plant and Cell Physiology. 1995;36:1303-1309.
821 60. Hatayama T, Takeno K. The metabolic pathway of salicylic acid rather than of chlorogenic acid is
822 involved in the stress-induced flowering of Pharbitis nil. J Plant Physiol. 2003;160:461-467.
823 61. Wang Y, Luo XJ, Sun F, Hu JH, Zha XJ, Su W, Yang JS. Overexpressing lncRNA LAIR increases grain yield
824 and regulates neighbouring gene cluster expression in rice. Nat Commun. 2018;9:3516.
825 62. Ghafouri-Fard S, Dashti S, Taheri M. The HOTTIP (HOXA transcript at the distal tip) lncRNA: Review of
826 oncogenic roles in human. Biomed Pharmacother. 2020;127.
827 63. Rigo R, Bazin J, Romero-Barrios N, Moison M, Lucero L, Christ A, Benhamed M, Blein T, Huguet S,
828 Charon C, et al. The Arabidopsis lncRNA ASCO modulates the transcriptome through interaction with
829 splicing factors. Embo Rep. 2020;21:e48977.
830 64. Bardou F, Ariel F, Simpson CG, Romero-Barrios N, Laporte P, Balzergue S, Brown JWS, Crespi M. Long
831 Noncoding RNA Modulates Alternative Splicing Regulators in Arabidopsis. Dev Cell. 2014;30:166-176.
832 65. Fonouni-Farde C, Ariel F, Crespi M. Plant Long Noncoding RNAs: New Players in the Field of Post-
833 Transcriptional Regulations. Non-Coding Rna. 2021;7:12.
834 66. Groff AF, Sanchez-Gomez DB, Soruco MML, Gerhardinger C, Barutcu AR, Li E, Elcavage L, Plana O,
835 Sanchez LV, Lee JC, et al. In vivo characterization of Linc-p21 reveals functional cis-regulatory DNA
836 elements. Cell Rep. 2016;16:2178-2186.
837 67. Paralkar VR, Taborda CC, Huang P, Yao Y, Kossenkov AV, Prasad R, Luan J, Davies JOJ, Hughes JR,
838 Hardison RC, et al. Unlinking an lncRNA from its associated cis element. Mol Cell. 2016;62:104-110.
839 68. Chen J, Brunner AD, Cogan JZ, Nunez JK, Fields AP, Adamson B, Itzhak DN, Li JY, Mann M, Leonetti MD,
840 Weissman JS. Pervasive functional translation of noncanonical human open reading frames. Science.
841 2020;367:1140-1146.
842 69. Lewandowski JP, Dumbovic G, Watson AR, Hwang T, Jacobs-Palmer E, Chang N, Much C, Turner KM,
843 Kirby C, Rubinstein ND, et al. The Tug1 lncRNA locus is essential for male fertility. Genome biology.
844 2020;21:237.
845 70. Chu C, Quinn J, Chang HY. Chromatin isolation by RNA purification (ChIRP). Journal of visualized
846 experiments : JoVE. 2012.
847 71. Raj A, van den Bogaard P, Rifkin SA, van Oudenaarden A, Tyagi S. Imaging individual mRNA molecules
848 using multiple singly labeled probes. Nat Methods. 2008;5:877-879.

72. Nelson ADL, Haug-Baltzell AK, Davey S, Gregory BD, Lyons E. EPIC-CoGe: managing and analyzing genomic data. Bioinformatics. 2018;34:2651-2653.
73. Lyons E, Freeling M. How to usefully compare homologous plant genes and chromosomes as DNA sequences. Plant Journal. 2008;53:661-673.
74. Geneious Prime. https://www.geneious.com. Accessed 2021.
75. Schneider CA, Rasband WS, Eliceiri KW. NIH Image to ImageJ: 25 years of image analysis. Nat Methods. 2012;9:671-675.
76. R Core Team. R: A language and environment for statistical computing. R Foundation for statistical computing, Vienna, Austria. https://www.R-project.org/. accessed.
77. GraphPad Prism 9. GraphPad Software, Inc. . http://www.graphpad.com Accessed 1 Jan 2021
78. Jin Y. FLAIL_2021. https://github.com/Yu-Jin-KU. Accessed 12 Aug 2021.
79. Andrews S. FastQC: a quality control tool for high throughput sequence data. http://www.bioinformatics.babraham.ac.uk/projects/fastqc. Accessed 18 Jan 2019.
80. Bolger AM, Lohse M, Usadel B. Trimmomatic: a flexible trimmer for Illumina sequence data. Bioinformatics. 2014;30:2114-2120.
81. Dobin A, Davis CA, Schlesinger F, Drenkow J, Zaleski C, Jha S, Batut P, Chaisson M, Gingeras TR. STAR: ultrafast universal RNA-seq aligner. Bioinformatics. 2013;29:15-21.
82. Li H, Handsaker B, Wysoker A, Fennell T, Ruan J, Homer N, Marth G, Abecasis G, Durbin R, Proc GPD. The Sequence Alignment/Map format and SAMtools. Bioinformatics. 2009;25:2078-2079.
83. Anders S, Huber W. Differential expression analysis for sequence count data. Genome biology. 2010;11:R106.
84. Krueger F. Trim Galore. https://github.com/FelixKrueger/TrimGalore. Accessed 23 Juy 2021.
85. Yu GC, Wang LG, He QY. ChIPseeker: an R/Bioconductor package for ChIP peak annotation, comparison and visualization. Bioinformatics. 2015;31:2382-2383.
86. Carlson MM, B.P. TxDb.Athaliana.BioMart.plantsmart28: Annotation package for TxDb object(s). https://bioconductor.org/packages/release/data/annotation/html/TxDb.Athaliana.BioMart.plantsmart28.html. Accessed 7 Oct 2015.
87. Robinson JT, Thorvaldsdottir H, Winckler W, Guttman M, Lander ES, Getz G, Mesirov JP. Integrative genomics viewer. Nature biotechnology. 2011;29:24-26.
88. Jin Y, Ivanov M, Marquardt S. GSE186215. https://www.ncbi.nlm.nih.gov/geo/query/acc.cgi?acc=GSE186215. Accessed 20 Oct 2021.

Fig. 1

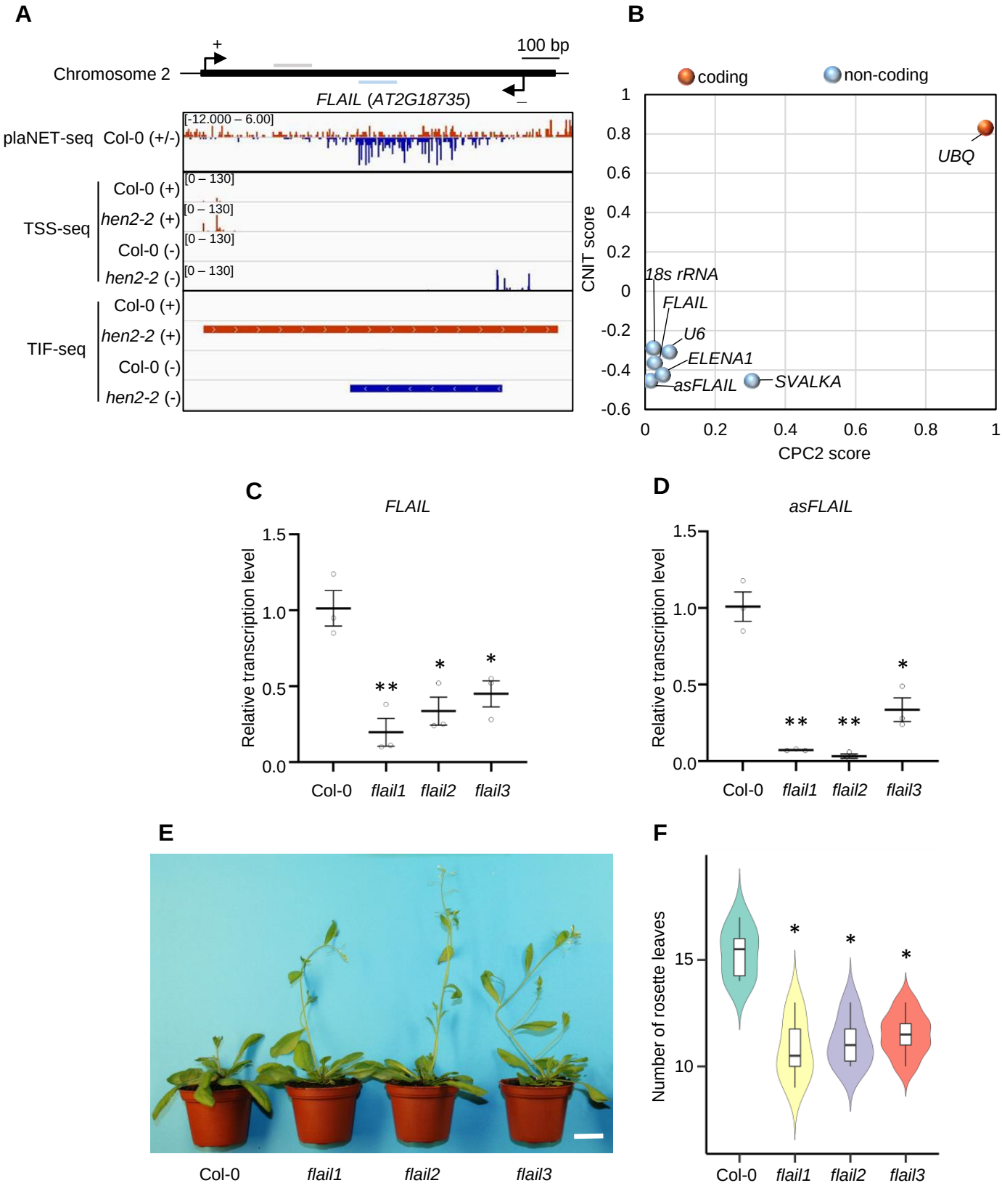

Fig. 1 Phenotypes of *FLAIL* knock-down plants. **A** Genome browser screenshot of plaNET-seq, TSS-seq and TIF-seq at the *FLAIL* genomic region in Col-0 and *hen2-2* mutant. Sense (+) and antisense (-) strands were shown in red and dark blue, respectively. Grey bar and light blue bar indicated primer locations of RT-qPCR for sense *FLAIL* (*FLAIL*) and antisense *FLAIL* (*asFLAIL*), respectively. **B** Coding potential of the transcript in the genomic region of *FLAIL* and *asFLAIL* and reference transcripts including non-coding RNAs (*18sRNA*, *U6*, *ELENA1*, *SVALKA*) and coding gene *UBQ* according to the CNIT and CPC2 algorithm. **C-D** Detection of *FLAIL* and *asFLAIL* gene expression in Col-0 and *flail* mutants by RT-qPCR. Transcript levels were normalized to *UBQ* expression levels. Y-axis showed relative values compared to the expression level of Col-0. Bars represented average ± s.e.m (n = 3 independent 14-d seedling pools). *, *p* value < 0.05 and **, *p* value < 0.01 by Student's t-test compared to Col-0. **E** Morphological phenotypes of 4-week-old plants of Col-0, *flail* mutants at 20 °C under a 16-h light/8-h dark growth condition. Scale bar: 2 cm. **F** Violin graph showed number of rosette leaves after appearance of the first flower bud in Col-0. Data represented the mean of six independent experiments. Boxes spanned the first to third quartile, bold black lines indicated median value for each group and whiskers represented the minimum and maximum values. *, *p* value < 0.05 was indicated by Student's t-test compared to Col-0.

Fig. 2

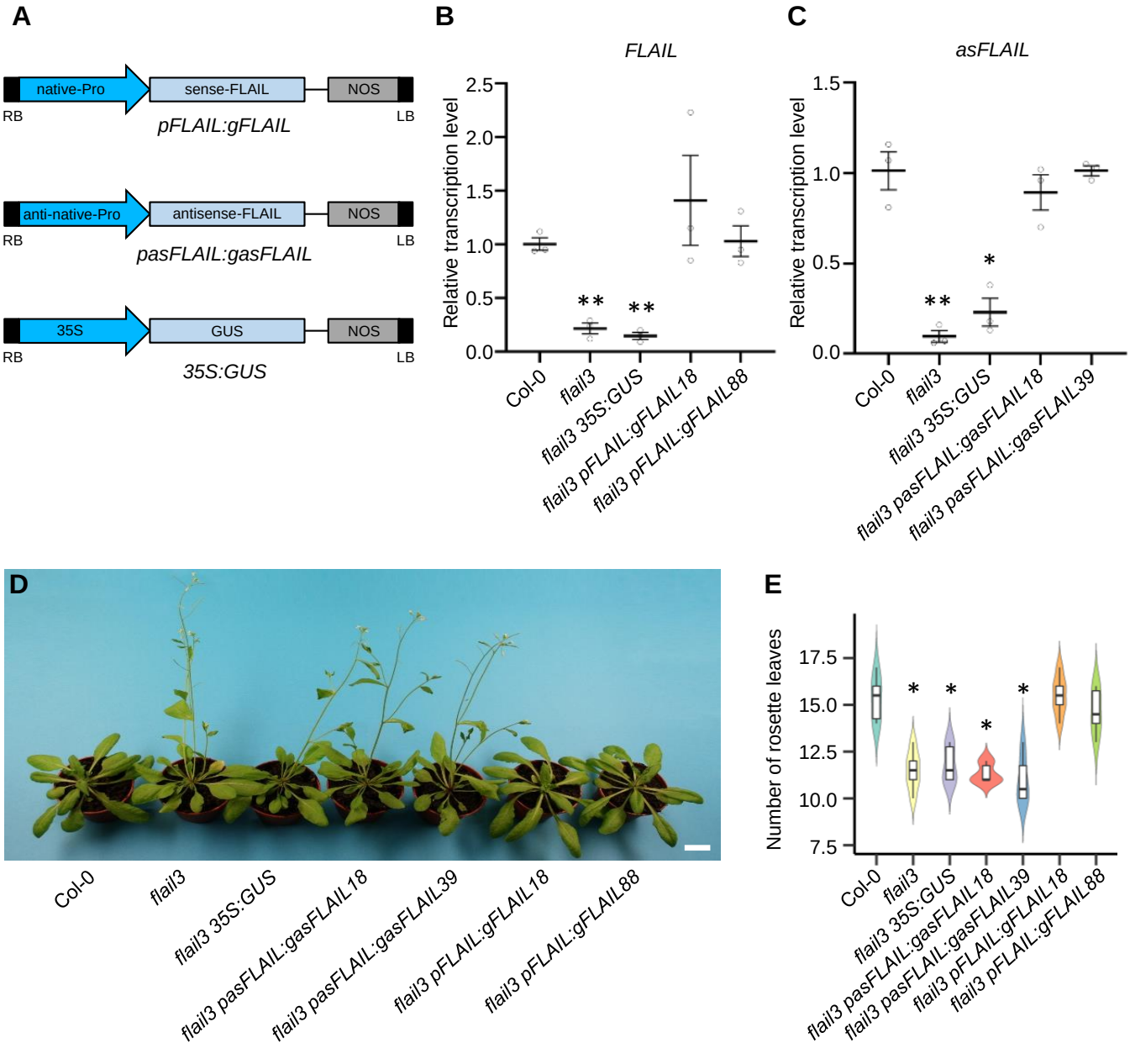

Fig. 2 *Sense-FLAIL* RNA is functional for flowering. **A** Schematic representations of the T-DNA constructs containing the native promoter of *sense-FLAIL* (native-Pro) fused to the *sense-FLAIL* DNA region with NOS as a terminator or the native promoter of *anti-sense FLAIL* (anti-native-Pro) fused to the *anti-sense FLAIL* DNA region or a negative control with the 35S promoter (35S) fused to GUS reporter were transformed into *flail3 Arabidopsis* plants. **B-C** Detection of *FLAIL* and *asFLAIL* genes expression in Col-0, *flail3* mutant and complemented lines expressing *pFLAIL:gFLAIL* and *pasFLAIL:gasFLAIL* by RT-qPCR. Transcript levels were normalized to *UBQ* expression levels. Y-axis showed relative values compared to the expression level of Col-0. Error bars represented s.e.m (n = 3 independent 14-d seedling pools). *, *p* value < 0.05 and **, *p* value < 0.01 by Student's t-test compared to Col-0. **D** Representative morphological phenotypes of 4-week-old plants of Col-0, *flail3* mutant, transgenic lines at 20 °C under a 16-h light/8-h dark growth condition. Scale bar: 2 cm. **E** Violin graph showed number of rosette leaves after appearance of the first flower bud in Col-0. Data represented the mean of six independent experiments. Boxes spanned the first to third quartile, bold black lines indicated median value for each group and whiskers represented the minimum and maximum values. *, *p* value < 0.05 was indicated by Student's t-test compared to Col-0.

Fig. 3

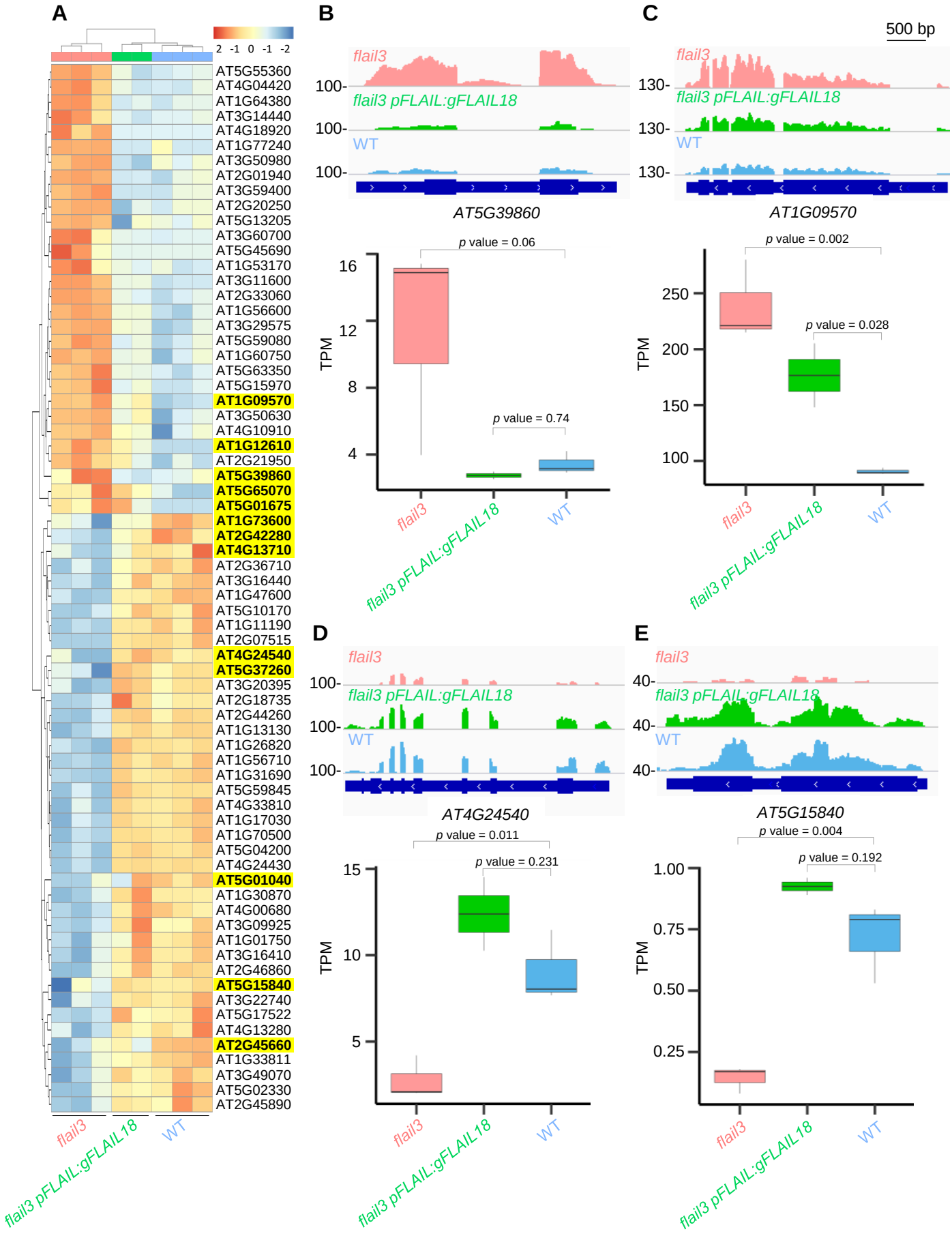

Fig. 3 *FLAIL* regulates flowering related genes. **A** Heatmap and hierarchical clustering of top 70 differentially expressed genes (DEGs) in *flail3 versus* Col-0 that were best rescued in the *flail3 pFLAIL:gFLAIL18* complementation line. DEGs analyzed by DESeq2 with |log2 fold change| > 1 and adjusted *p* value < 0.05 were considered significant differential expression. Three biological replicates for *flail3*, wild type, and two for *flail3 pFLAIL:gFLAIL18.* Flowering genes were highlighted in yellow bold. Samples clustered together on the basis of corresponding similar expression profiles. The color scale reflected the log 2-fold change in gene expression, ranging from down-regulated (blue) to up-regulated (red). **B-E** Genome browser screenshots illustrating the expression of dysregulated flowering genes in *flail3* were rescued in complementation line (top panel). Normalized read counts (TPM from RNA-seq) for differentially expressed flowering genes in WT, *flail3*, and *flail3 pFLAIL:gFLAIL18* plants (bottom panel). Boxes spanned the first to third quartile, bold black lines indicated median value for each group and whiskers represented the minimum and maximum values. All *p* values were denoted by Students' t-test. Bar = 500 bp.

Fig. 4

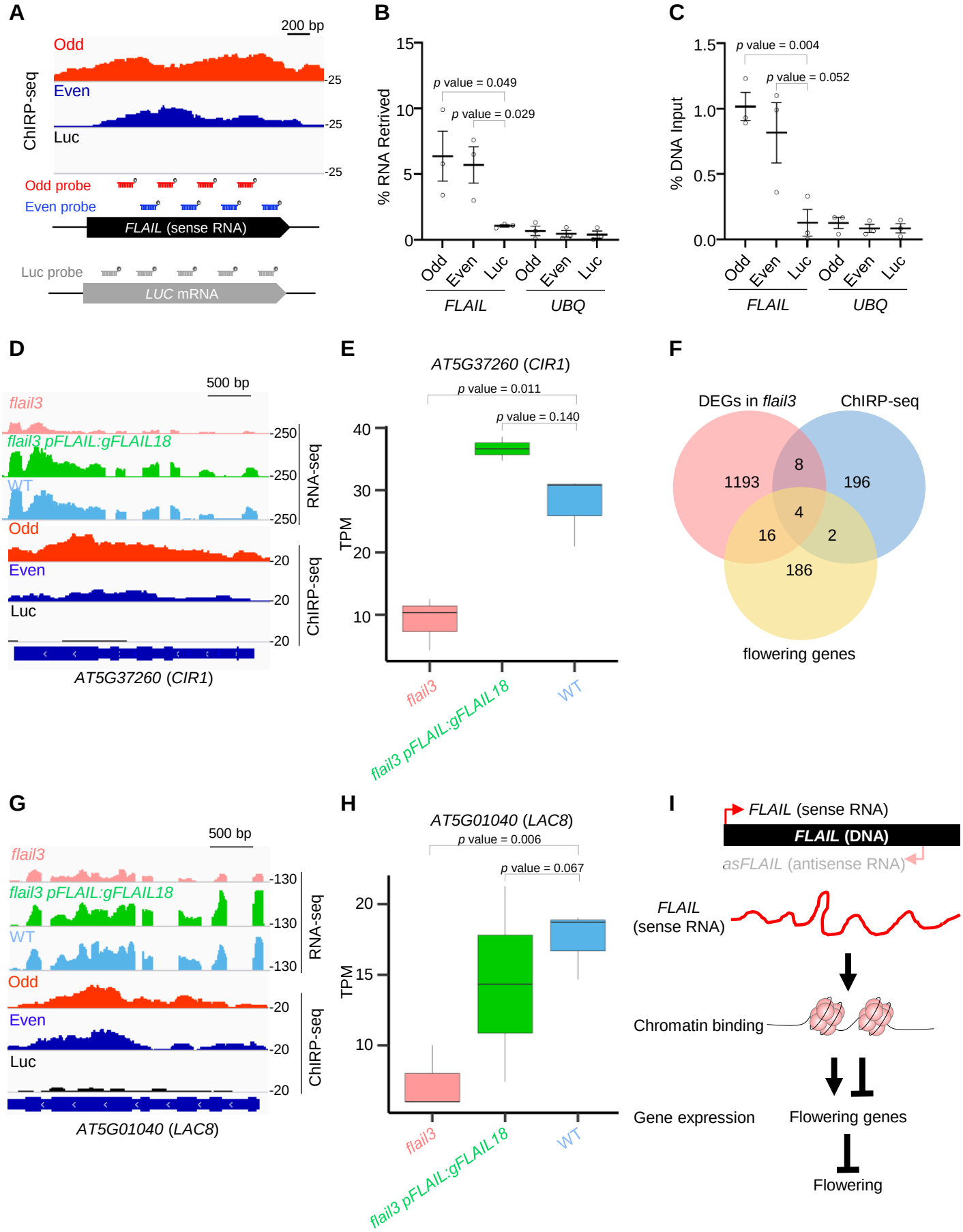

Fig. 4 *FLAIL* affects flowering by chromatin binding of flowering genes. **A** Top, *FLAIL* bound the locus itself by ChIRP-seq from two independent Odd and Even probed chromatins. Luc probe was used as a control. Bottom, schematic representation of the antisense oligonucleotide probes that were biotinylated at the 3′-end with Odd (in red) and Even (in dark blue) against *FLAIL* sense RNA and Luc probe (in grey) against *LUC* mRNA. **B** ChIRP-qPCR using probe pools *FLAIL*-asDNA (Odd and Even) retrieved ~5%–10% of *FLAIL* endogenous RNA and < 1% levels of *UBQ*. *Luc*-asDNA probes retrieved much lower levels of both RNAs as a control. **C** *FLAIL* DNA signal was identified in both Odd and Even probes. *UBQ* region showed much less binding signal in all probes as a negative control. Graphs in **B** & **C** showed the mean ± s.e.m. (n= 3 independent replicates). **D, G** Genome browser screenshots illustrating two of *FLAIL* bound targets *CIR1* (**D**) and *LAC8* (**G**) in RNA-seq (lane 1-3) and ChIRP-seq (lane 4-6). FLAIL binding peaks were called by CCAT3.0 with the cutoff FDR = 0.232. **E, H** Normalized read counts (TPM from RNA-seq) for differentially expressed (DE) flowering genes in WT, *flail3*, and *flail3 pFLAIL:gFLAIL18* plants (bottom panel). Boxes spanned the first to third quartile, bold black lines indicated median value for each group and whiskers represented the minimum and maximum values. **F** Venn diagram of genes targeted by *FLAIL* (ChIRP-seq) and genes overlapped with DEGs in *flail3* and flowering related genes. **I** A model for the *trans*-acting *FLAIL* sense RNA regulated flowering. The *FLAIL* sense RNA binds chromatin regions of flowering genes to regulate expression levels of flowering related genes and thus affects flowering time. All *p* values were denoted by Students' t-test.

A

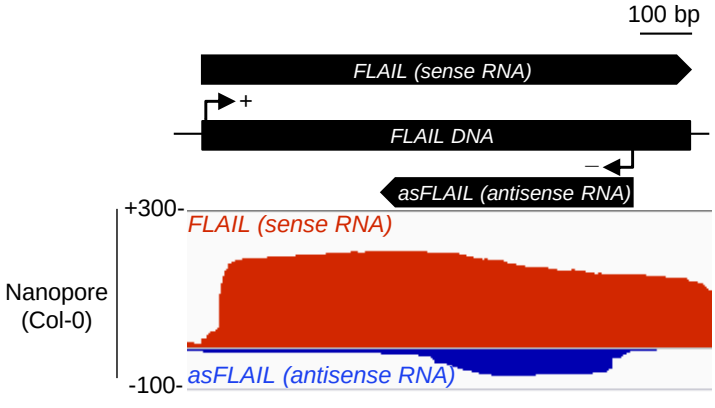

B

AAGTTAATAAACCACACAAAAAAGTTTTTCTCTCTTCGCTCTCTCGTAGTTTGTAAAGATAGAAACTGAAATTTCTTTTGTTTTTGTTAACCGG
ATAGTTTTCCGGTGAGTCGCCGTCCCGTTTAATTCGGGCTTTCGTCCGACATCTTCTAGCTACGTTAGTGGAGATGGTTGGCTTTTTGTATGGC
ATCGTTGGCTAACTTAGCGACGTTGGCCAGCTTCCGTACGGCAGCGTTGGGCTTACACTAACAGCGTTGGTCATCTTTGTTTTTGTTTTGTTAC
TTCAAAGGTTTGATGATGAAGCTTTATGGCATGCAGAATCGTCAGATCTGAAGAGGGTTTCTCTTTACAAGATCTATTCTCCTTCTGTTTTGTT
TAGCTTCACTATTGGGTTATGCTTTTGGCTCTGGTAGTTTTTCGGCGATGTGTGCGTTTCCAGCAATTACCCTCGTTTGGATCTACCATATTTA
AGACAGTTTCAATTTTATTTTCGCCTAAGATTGGGTTAAAGCTTCTATCCTATGCAAATTTGATATGCCTTTAGTGCTTTTGCAAGAGAGTTCG
AAGATTCAATGGTTGGACAAGTTTGAACTACTCAATTTTTTTAATTTCTTTACCCGTTTTGATGAATTATTTGTGATTCTAGCAACCATATGAG
ATTAGGAAATTGATGTTTGTTCTATAACATCTAATTGCCATAATCGGTGATAGAAAAAAAGAGTTTCATTGCTCGGTGCTTTCCCGGCGATGGT
TCTCCGATTCACCAGACTTGAGTCTCATCCGGTGGAGGTTGTGGAAGATTCACGTGTCCTTAGCTTATTATTATTGGTCTGACACGTCTTAAGC
TTATCTCTTTTTTGTGACGTAAAAGTCTGTTGTGGACCTCATATGTAGACTGTCTTGAGCCTTTTATGTTGTAACACTGAGCCTCAGTATATTA
AAAATAAATCTTTCTCTG

Fig. S1 Characterization of *FLAIL* locus. **A** Genome browser view of *FLAIL* splicing status in nanopore sequencing of Col-0. Transcription of sense *FLAIL* RNA and *asFLAIL* RNA were shown in red and dark blue, respectively and no isoform resulting from alternative splicing was observed. **B** *FLAIL* nucleotide sequences in black and two sORFs locations in blue.

Fig. S2

NetStart Prediction

```
Name: FLAIL
AAGTTAATAAACCACACAAAAAAGTTTTTCTCTCTTCG
CTCTCTCGTAGTTTGTAAAGATAGAAACTGAAATTTCT
TTTGTTTTTGTTAACCGGATAGTTTTCCGGTGAGTCGC
CGTCCCGTTTAATTCGGGCTTTCGTCCGACATCTTCTA
GCTACGTTAGTGGAGATGGTTGGCTTTTTGTATGGCAT
CGTTGGCTAACTTAGCGACGTTGGCCAGCTTCCGTACG
GCAGCGTTGGGCTTACACTAACAGCGTTGGTCATCTTT
GTTTTTGTTTTGTTACTTCAAAGGTTTGATGATGAAGC
TTTATGGCATGCAGAATCGTCAGATCTGAAGAGGGTTT
CTCTTTACAAGATCTATTCTCCTTCTGTTTTGTTTAGC
TTCACTATTGGGTTATGCTTTTGGCTCTGGTAGTTTTT
CGGCGATGTGTGCGTTTCCAGCAATTACCCTCGTTTGG
ATCTACCATATTTAAGACAGTTTCAATTTTATTTTCGC
CTAAGATTGGGTTAAAGCTTCTATCCTATGCAAATTTG
ATATGCCTTTAGTGCTTTTGCAAGAGAGTTCGAAGATT
CAATGGTTGGACAAGTTTGAACTACTCAATTTTTTTAA
TTTCTTTACCCGTTTTGATGAATTATTTGTGATTCTAG
CAACCATATGAGATTAGGAAATTGATGTTTGTTCTATA
ACATCTAATTGCCATAATCGGTGATAGAAAAAAAGAGT
TTCATTGCTCGGTGCTTTCCCGGCGATGGTTCTCCGAT
TCACCAGACTTGAGTCTCATCCGGTGGAGGTTGTGGAA
GATTCACGTGTCCTTAGCTTATTATTATTGGTCTGACA
CGTCTTAAGCTTATCTCTTTTTTGTGACGTAAAAGTCT
GTTGTGGACCTCATATGTAGACTGTCTTGAGCCTTTTA
TGTTGTAACACTGAGCCTCAGTATATTAAAAATAAATC
TTTCTCTG
......................................
......................................
......................................
......................................
...............N...............N......
......................................
......................................
............................N..N......
...N....N.............................
......................................
..............N.......................
.....N................................
......................................
...........................N..........
..N...................................
..N...................................
.................N....................
.......N................N.............
......................................
.........................N............
......................................
......................................
......................................
..............N......................N
......................................
........
```

Pos	Score	Pred
168	0.419	-
184	0.218	-
295	0.106	-
298	0.149	-
308	0.366	-
313	0.287	-
395	0.318	-
424	0.324	-
522	0.290	-
535	0.346	-
573	0.305	-
626	0.262	-
654	0.199	-
671	0.443	-
748	0.208	-
889	0.080	-
912	0.048	-

```
Name: UBQ10
TCGTGTTTATCAACTCAAAGCACAAATACTTTTCCTCAACCTAAAAATAAGGCAATTAGCCAAAAACAACTTTGCGTGTAAACAACGCTCAATACAC
GTGTCATTTTATTATTAGCTATTGCTTCACCGCCTTAGCTTTCTCGTGACCTAGTCGTCCTCGTCTTTTCTTCTTCTTCTTCTATAAAACAATACCC
AAAGAGCTCTTCTTCTTCACAATTCAGATTTCAATTTCTCAAAATCTTAAAAACTTTCTCTCAATTCTCTCTACCGTGATCAAGGTAAATTTCTGTG
TTCCTTATTCTCTCAAAATCTTCGATTTTGTTTTCGTTCGATCCCAATTTCGTATATGTTCTTTGGTTTAGATTCTGTTAATCTTAGATCGAAGACG
ATTTTCTGGGTTTGATCGTTAGATATCATCTTAATTCTCGATTAGGGTTTCATAGATATCATCCGATTTGTTCAAATAATTTGAGTTTTGTCGAATA
ATTACTCTTCGATTTGTGATTTCTATCTAGATCTGGTGTTAGTTTCTAGTTTGTGCGATCGAATTTGTCGATTAATCTGAGTTTTTCTGATTAACAG
ATGCAGATCTTTGTTAAGACTCTCACCGGAAAGACAATCACCCTCGAGGTGGAAAGCTCCGACACCATCGACAACGTTAAGGCCAAGATCCAGGATA
AGGAGGGCATTCCTCCGGATCAGCAGAGGCTTATTTTCGCCGGCAAGCAGCTAGAGGATGGCCGTACGTTGGCTGATTACAATATCCAGAAGGAATC
CACCCTCCACTTGGTCCTCAGGCTCCGTGGTGGTATGCAGATTTTCGTTAAAACCCTAACGGGAAAGACGATTACTCTTGAGGTGGAGAGTTCTGAC
ACCATCGACAACGTCAAGGCCAAGATCCAAGACAAAGAGGGTATTCCTCCGGACCAGCAGAGGCTGATCTTCGCCGGAAAGCAGTTGGAGGATGGCA
GAACTCTTGCTGACTACAATATCCAGAAGGAGTCCACCCTTCATCTTGTTCTCAGGCTCCGTGGTGGTATGCAGATTTTCGTTAAGACGTTGACTGG
GAAAACTATCACTTTGGAGGTGGAGAGTTCTGACACCATTGATAACGTGAAAGCCAAGATCCAAGACAAAGAGGGTATTCCTCCGGACCAGCAGAGA
TTGATCTTCGCCGGAAAACAACTTGAAGATGGCAGAACTTTGGCCGACTACAACATTCAGAAGGAGTCCACACTCCACTTGGTCTTGCGTCTGCGTG
GAGGTATGCAGATCTTCGTGAAGACTCTCACCGGAAAGACCATCACTTTGGAGGTGGAGAGTTCTGACACCATTGATAACGTGAAAGCCAAGATCCA
GGACAAAGAGGGTATCCCACCGGACCAGCAGAGATTGATCTTCGCCGGAAAGCAACTTGAAGATGGAAGAACTTTGGCTGACTACAACATTCAGAAG
GAGTCCACACTTCACTTGGTCTTGCGTCTGCGTGGAGGTATGCAGATCTTCGTGAAGACTCTCACCGGAAAGACTATCACTTTGGAGGTAGAGAGCT
CTGACACCATTGACAACGTGAAGGCCAAGATCCAGGATAAGGAAGGAATCCCTCCGGACCAGCAGAGGTTGATCTTTGCCGGAAAACAATTGGAGGA
TGGTCGTACTTTGGCGGATTACAACATCCAGAAGGAGTCGACCCTTCACTTGGTGTTGCGTCTGCGTGGAGGTATGCAGATCTTCGTCAAGACTTTG
ACCGGAAAGACCATCACCCTTGAAGTGGAAAGCTCCGACACCATTGACAACGTCAAGGCCAAGATCCAGGACAAGGAAGGTATTCCTCCGGACCAGC
AGCGTCTCATCTTCGCTGGAAAGCAGCTTGAGGATGGACGTACTTTGGCCGACTACAACATCCAGAAGGAGTCTACTCTTCACTTGGTCCTGCGTCT
TCGTGGTGGTTTCTAAATCTCGTCTCTGTTATGCTTAAGAAGTTCAATGTTTCGTTTCATGTAAAACTTTGGTGGTTTGTGTTTTGGGGCCTTGTAT
AATCCCTGATGAATAAGTGTTCTACTATGTTTCCGTTCCTGTTATCTCTTTCTTTCTAATGACAAGTCGAACTTCTTCTTTATCATCGCTTCGTTTT
TATTATCTGTGCTTCTTTTGTTTAATACGCCTGCAAAGTGACTCGACTCTGTTTAGTGCAGTTCTGCGAAACTTGTAAATAGTCCAATTGTTGGCCT
CTAGTAATAGATGTAGCGAAAGTGTTGAGCTGTTGGGTTCTAAGGATGGCTTGAACATGTTAATCTTTTAGGTTCTGAGTATGATGAACATTCGTTG
TTGC
.................................................................................................
.................................................................................................
.................................................................................................
.......................................................N.........................................
.................................................................................................
.................................................................................................
i................................................................................................
.........................................................N.......................................
..................................i..............................................................
...........................................................................................N.....
....................................................................N............................
.................................................................................................
............................N....................................................................
.....i...........................................................................................
..............................................................N..................................
.......................................i.........................................................
................................................................................................N
.........................................................................i.......................
.................................................................................................
.................................N...............................................................
..............................N...............N...........N......................................
........N.................N...............................N......................................
.................................................................................................
................................................................................................
....
```

Pos	Score	Pred
347	0.377	-
583	0.718	Yes
737	0.265	-
811	0.543	Yes
965	0.126	-
1039	0.471	-
1193	0.355	-
1267	0.549	Yes
1421	0.257	-
1495	0.537	Yes
1649	0.192	-
1723	0.667	Yes
1877	0.200	-
1971	0.188	-
1987	0.057	-
1999	0.152	-
2046	0.181	-
2064	0.345	-
2096	0.241	-
2242	0.100	-
2277	0.111	-
2288	0.054	-
2312	0.042	-
2315	0.038	-

Fig. S2 Assessment of *FLAIL* and *UBQ* for protein coding potential. Initiation codon translational analysis using NetStart for *FLAIL* and *UBQ*. The predicted initiation codons were depicted with the letter i, other instances of "ATG" by the letter "N" (non-start). The dots (".") were place holders for all the other sequence elements. The scores were always in [0.0, 1.0]; when greater than 0.5, they represented a probable translation start.

Fig. S3

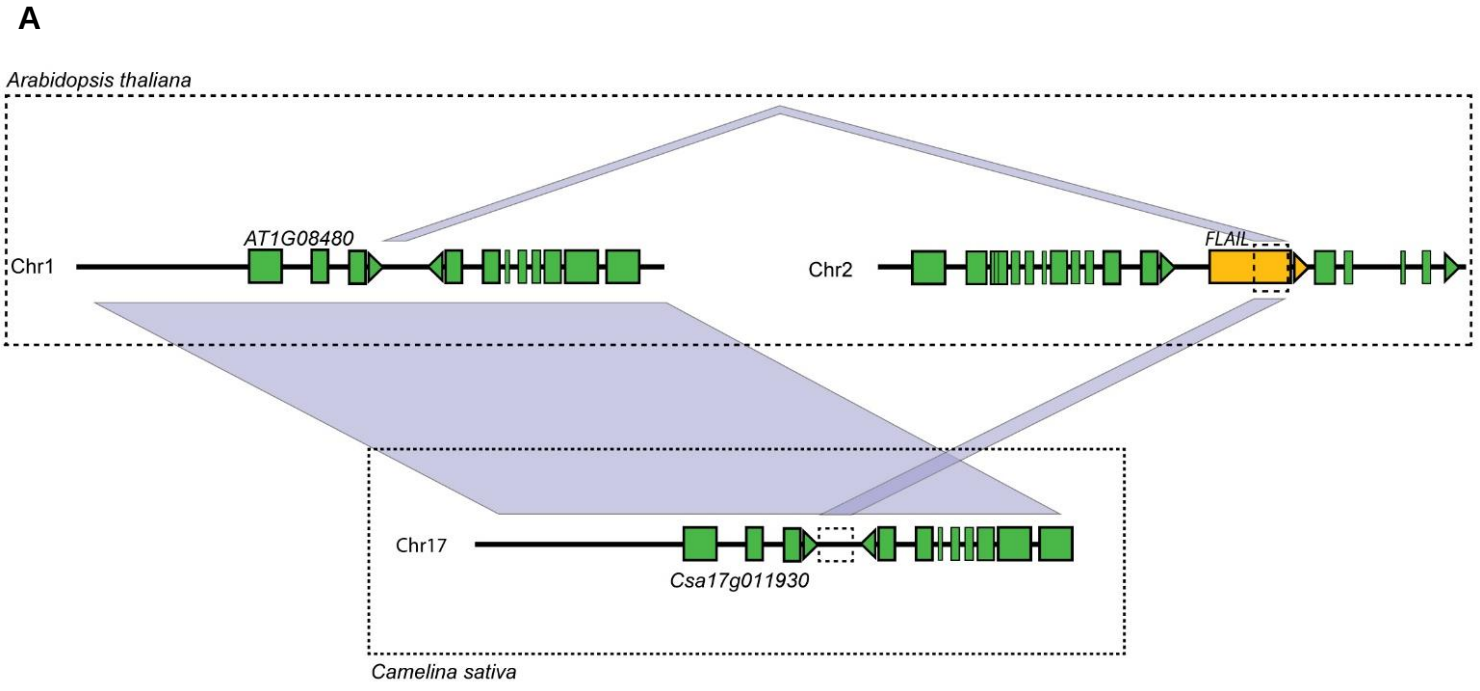

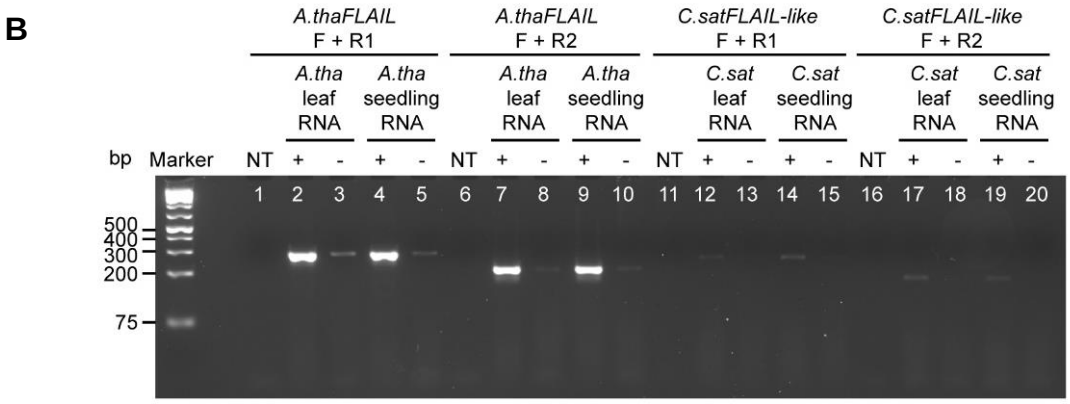

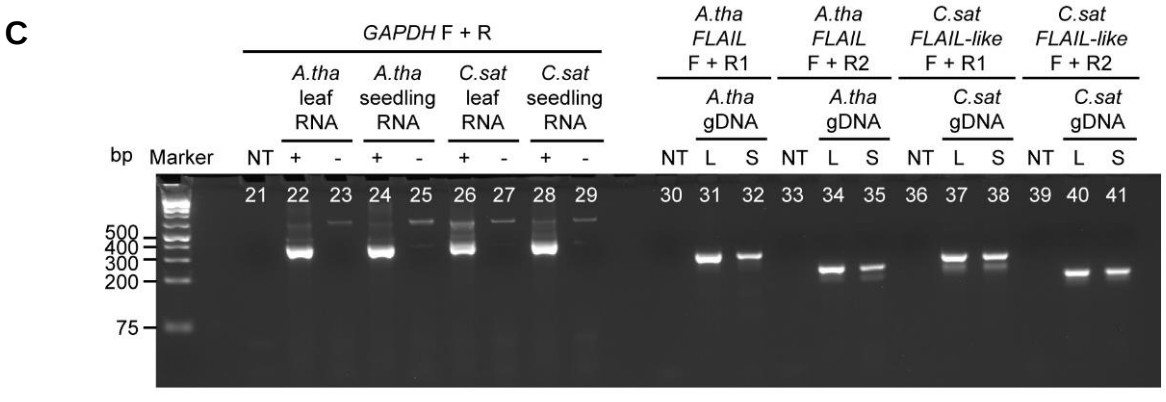

Fig. S3 Sequence and transcriptional conservation at the *FLAIL* and *FLAIL-like* loci in *Arabidopsis* and *Camelina*. **A** Schematic depicting the conservation of the *Arabidopsis* (*A.tha*) *FLAIL* locus in *Camelina sativa* (*C.sat*). Green boxes represent exons, with triangles representing direction of transcription. The *FLAIL* locus is represented by a yellow box. Faded blue lines represent sequence similarity between different loci. Dashed boxes at the *FLAIL* and *Csa17g011930* loci represent regions targeted for RT-PCR. **B** Amplification of *A.thaFLAIL* and *C.satFLAIL*-like, using RNA template (+/- RT, lanes 1-20). NT indicates no template was added to the reaction. **C** Control amplifications: *GAPDH* was amplified using RNA template (+/- RT, lanes 21-29), and *A.thaFLAIL* and *C.satFLAIL-like* were amplified using genomic DNA template (lanes 30-41). L indicates leaf tissue, S indicates seedling tissue.

Fig. S4

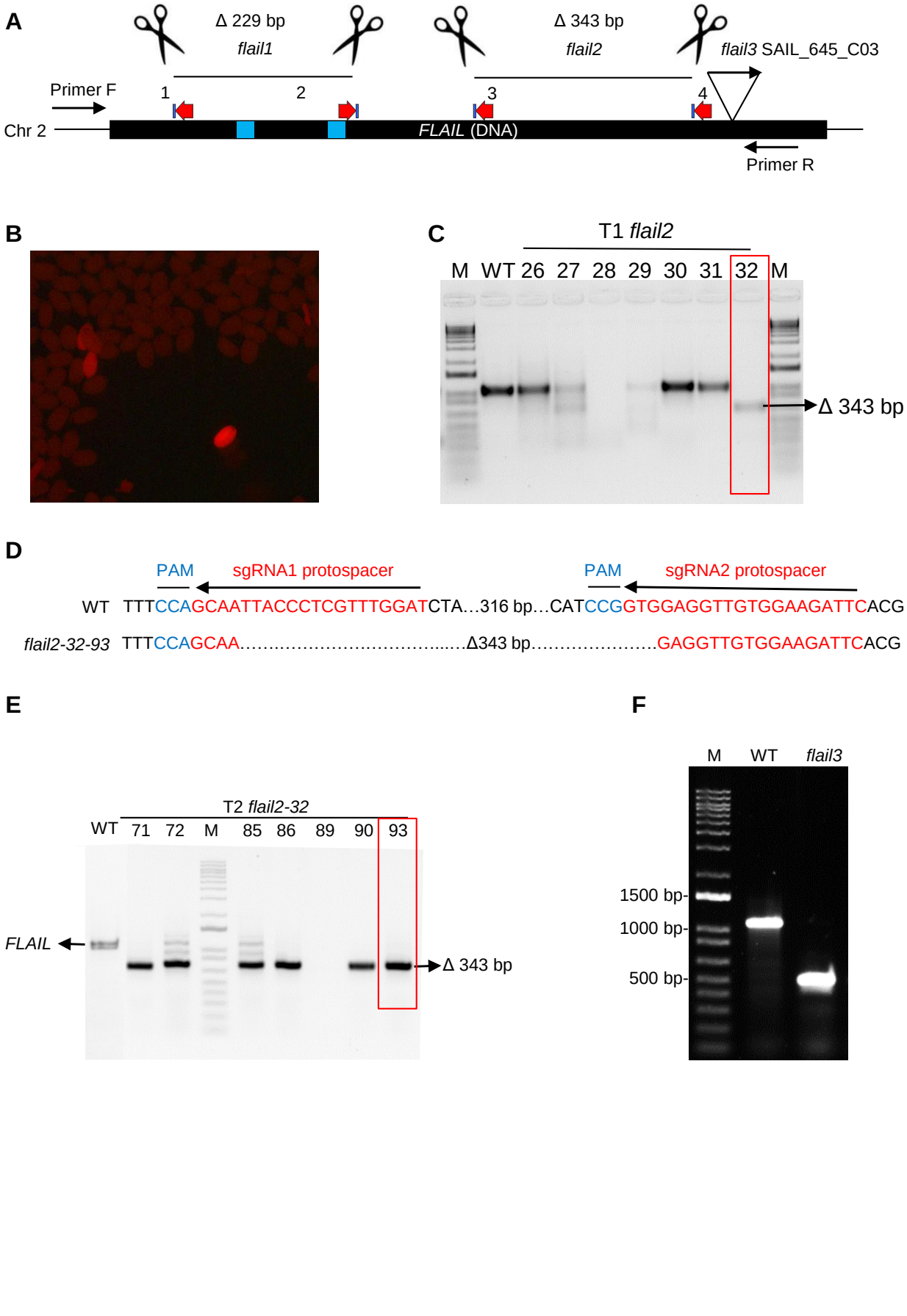

Fig. S4 *FLAIL* dual-sgRNA approach and T-DNA insertion genotyping. **A** Schematic representation of targeted gene *FLAIL* with locations of two Cas9-directed mutants *flail1*, *flail2*, and one T-DNA mutant *flail3*. Locations of dual-sgRNA target sites were shown in red arrow, primer pair F/R (Mlo2478/2479) were used for PCR testing deletion in *flail1* and *flail2*, triangle indicated the putative position of T-DNA insertion at the *FLAIL* locus. Blue boxes indicated two sORFs. **B** Similar to the previous generation of *flail1*, *FLAIL2* construct containing pKIR1.1 enabled red fluorescence selection of *flail2* seeds from T1 plants after transformation by floral dipping. **C** Genotyping of individual T1 plant with red fluorescence, Leaf genomic DNA of T1 plants were PCR amplified. Expected size of PCR product for deletion was 343 bp in *flail2* line. *flail2-32* in red box was selected for next generation. **D** In T2 selection, the null mutant *flail2-32-93* without red fluorescence in seeds represented Cas9-free plants, indicated by red box in **E**. PAM was shown in blue, sgRNA protospacers were in red, and deleted bases were replaced by dots. **E** PCR analysis of T2 lines. The expected size of the wild-type *FLAIL* amplicon and the deletion size between Cas9 cut sites in *flail2-32-93* were indicated. This inherited Cas9-null segregation line was used for data analysis in Fig. 1. **F** Genotyping of the T-DNA insertion mutant *flail3*. Gel sample order (from left to right): lane 1, marker; lane 2, WT; lane 3, *flail3*, with primer set, Mlo1788 + Mlo1789 + Mlo37; Results clearly showed that *flail3* line was homozygous since WT was the only line giving WT band and *flail3* line gave the only T-DNA insertion band.

Fig. S5

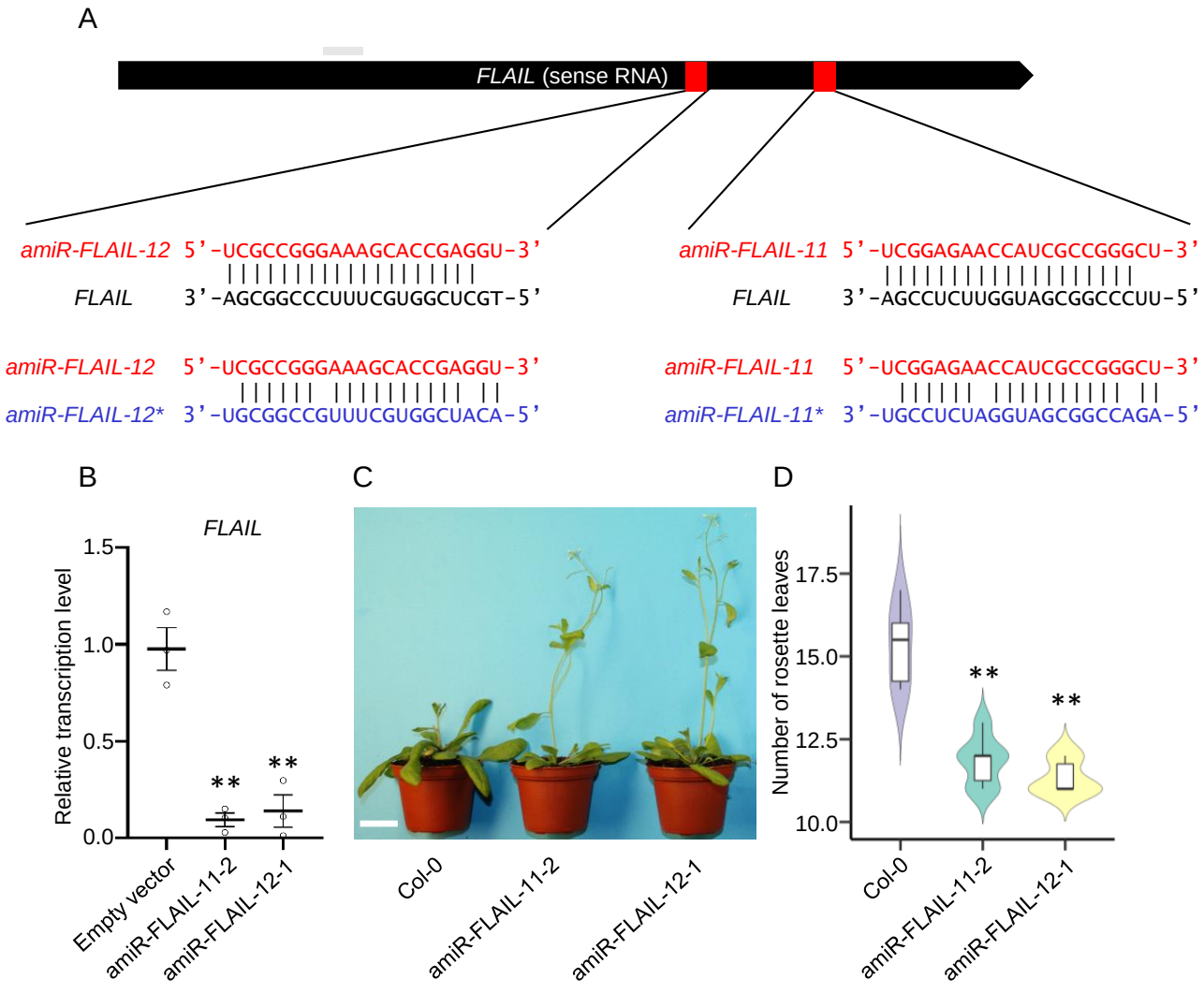

Fig. S5 *FLAIL* lncRNA functions as a flowering repressor. **A** Sequences and structures of amiRNA duplexes and the target sites of *amiR-FLAILs* and *amiR-FLAIL*s*. Upper panel, schematic representation of transcribed sense *FLAIL* RNA. Lower panel, sequences of amiRNA duplexes, amiRNA (in red) target sites, and potential amiRNA* (in blue) on cognate sense *FLAIL* (in black). **B** Gene expression of *sense FLAIL* in *amiR-FLAIL* plants by RT-qPCR. Transcript levels were normalized to *UBQ* expression levels. Two representative lines for amiRNA designed transgenic plants were selected. Y-axis showed relative values compared to the expression level of empty vector transformed plants. Grey bars depicted the relative positions of primers used for RT-qPCR analyses. Transcript levels were normalized to *UBQ* expression levels. Error bars represented s.e.m (n = 3 independent 14-day seedling pools). **, *p* value < 0.01 analyzed by Student's t-test. **C** Morphological phenotypes of 4-week-old plants of Col-0 and two *amiR-FLAIL* plants under a 16-h light/8-h dark growth condition. Scale bar: 2 cm. **D** Violin graph showed number of rosette leaves after appearance of the first flower bud in Col-0. Data represented the mean of six independent experiments. Boxes spanned the first to third quartile, bold black lines indicated median value for each group and whiskers represented the minimum and maximum values. **, *p* value < 0.01 was indicated by Student's t-test compared to Col-0.

Fig. S6

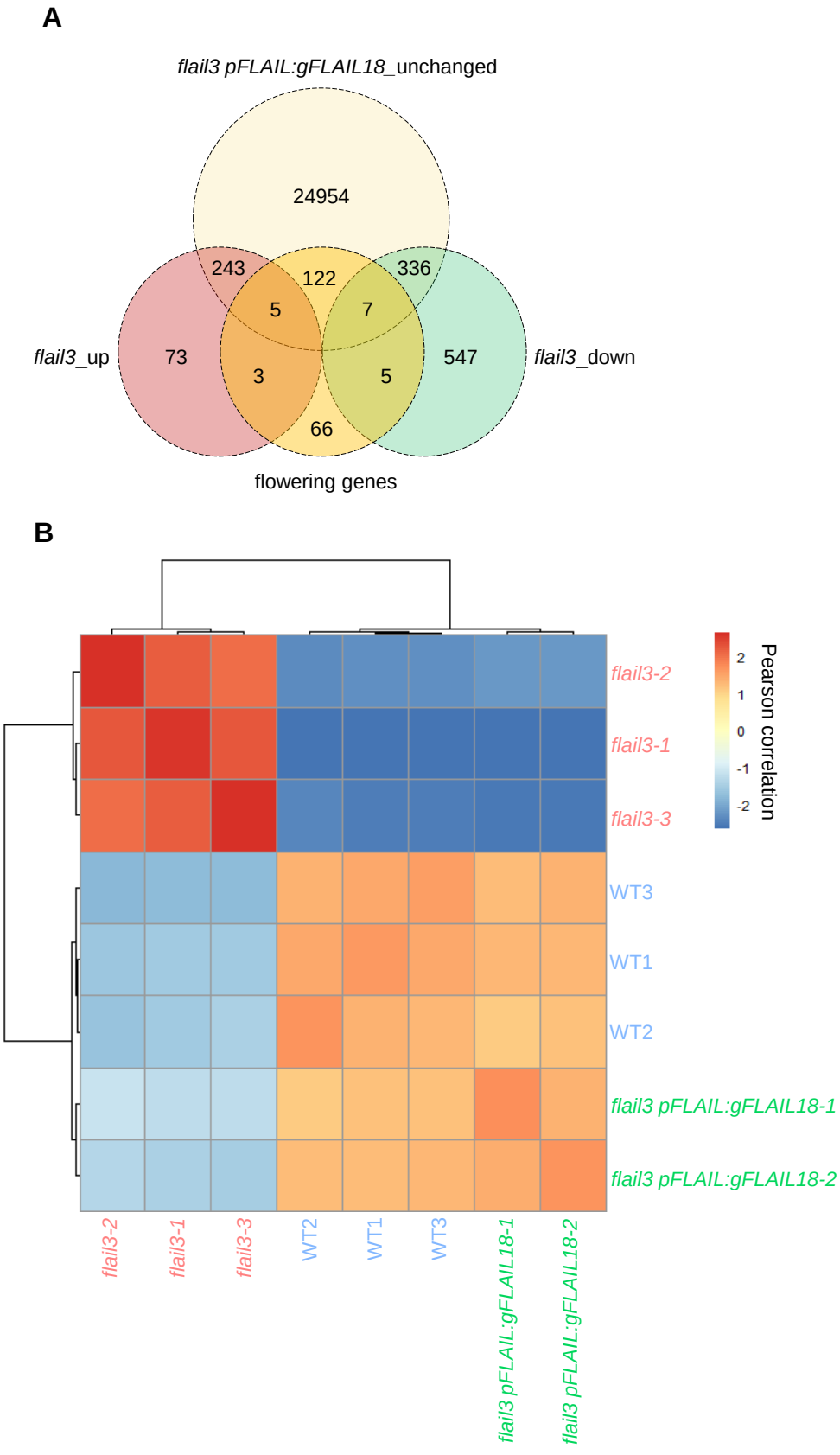

Fig. S6 Genome-wide effects of *FLAIL* on gene expression by RNA-seq. **A** Venn diagram of flowering genes overlapped with upregulated and downregulated genes in the *flail3* mutant and with unchanged genes in the *flail3 pFLAIL:gFLAIL18* complementation plant. **B** Reproducibility of all genes shown in Fig. 3 from RNA-seq data was demonstrated by clustered heatmap of Pearson correlation coefficients over all independent replicates of RNA-seq in WT, *flail3* mutant, and *flail3 pFLAIL gFLAIL18* plants. Darker red denoted higher correlation and darker blue represented low reproducibility.

Fig. S7

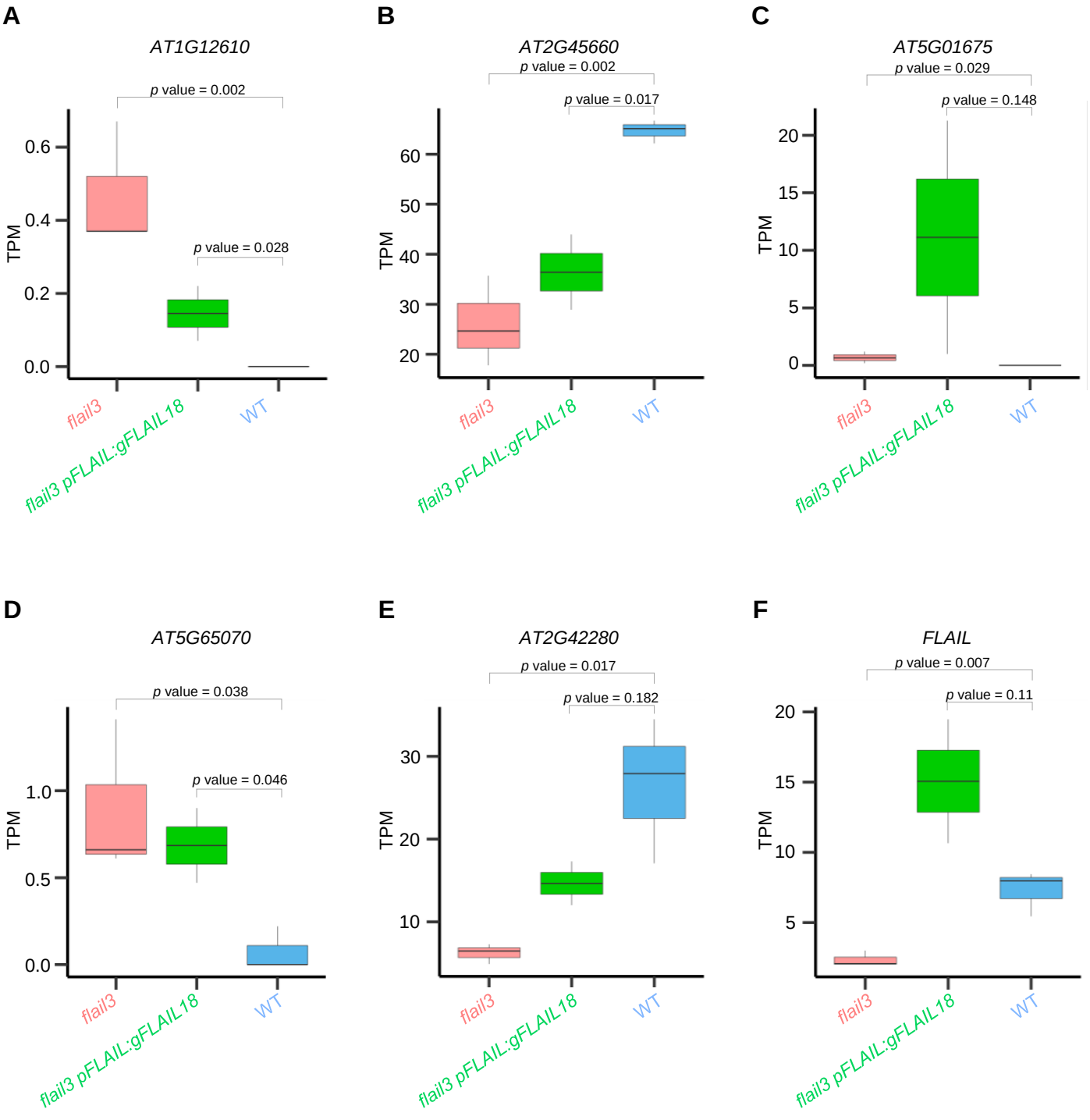

Fig. S7 *FLAIL* regulates flowering related genes in *trans.* **A-F** Genome browser screenshots illustrating the expression of dysregulated flowering genes in *flail3* were most fully rescued in complementation line. Normalized read counts (TPM from RNA-seq) were used for differentially expressed flowering genes in WT, *flail3*, and *flail3 pFLAIL:gFLAIL18* plants. Boxes spanned the first to third quartile, bold black lines indicated median value for each group and whiskers represented the minimum and maximum values. *p* value was denoted by Students' t-test.

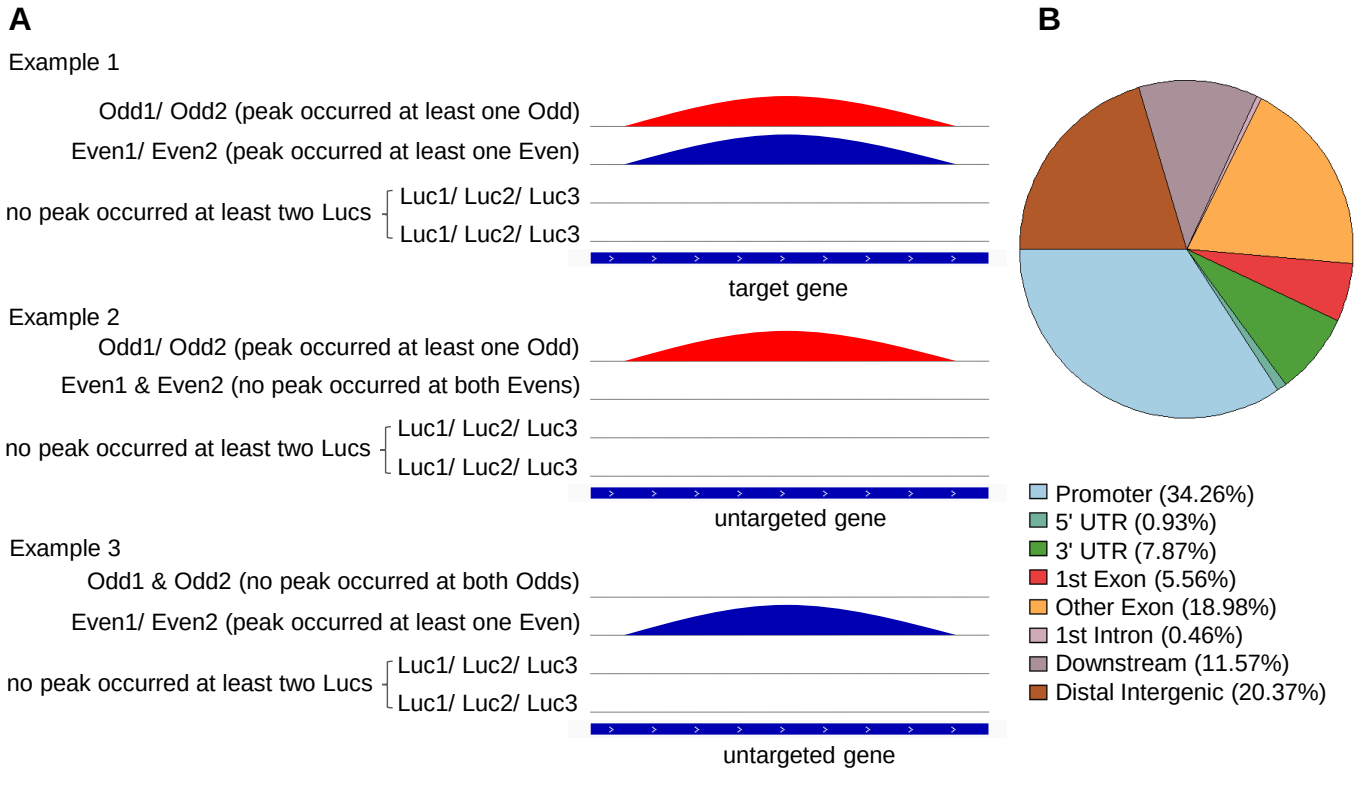

Fig. S8 Strategy to identify genome-wide binding profile of *FLAIL* analyzed by ChIRP-seq. **A** Illustration of *FLAIL* peaks called by CCAT3.0. Only peaks that occurred at target genes from both Even and Odd probed DNA, but not from two or more independent experiments of Luc pools were considered significant enrichment (Example 1), peaks that only occurred from either Even or Odd pools were not considered *FLAIL* targets (Example 2 & 3). **B** A pie chart that was generated by ChIPseeker represented distribution of *FLAIL* bound regions in the genome. A total of 210 *FLAIL* bound regions were annotated according to the genomic distribution and *FLAIL* was enriched predominantly in promoter regions.

Fig. S9

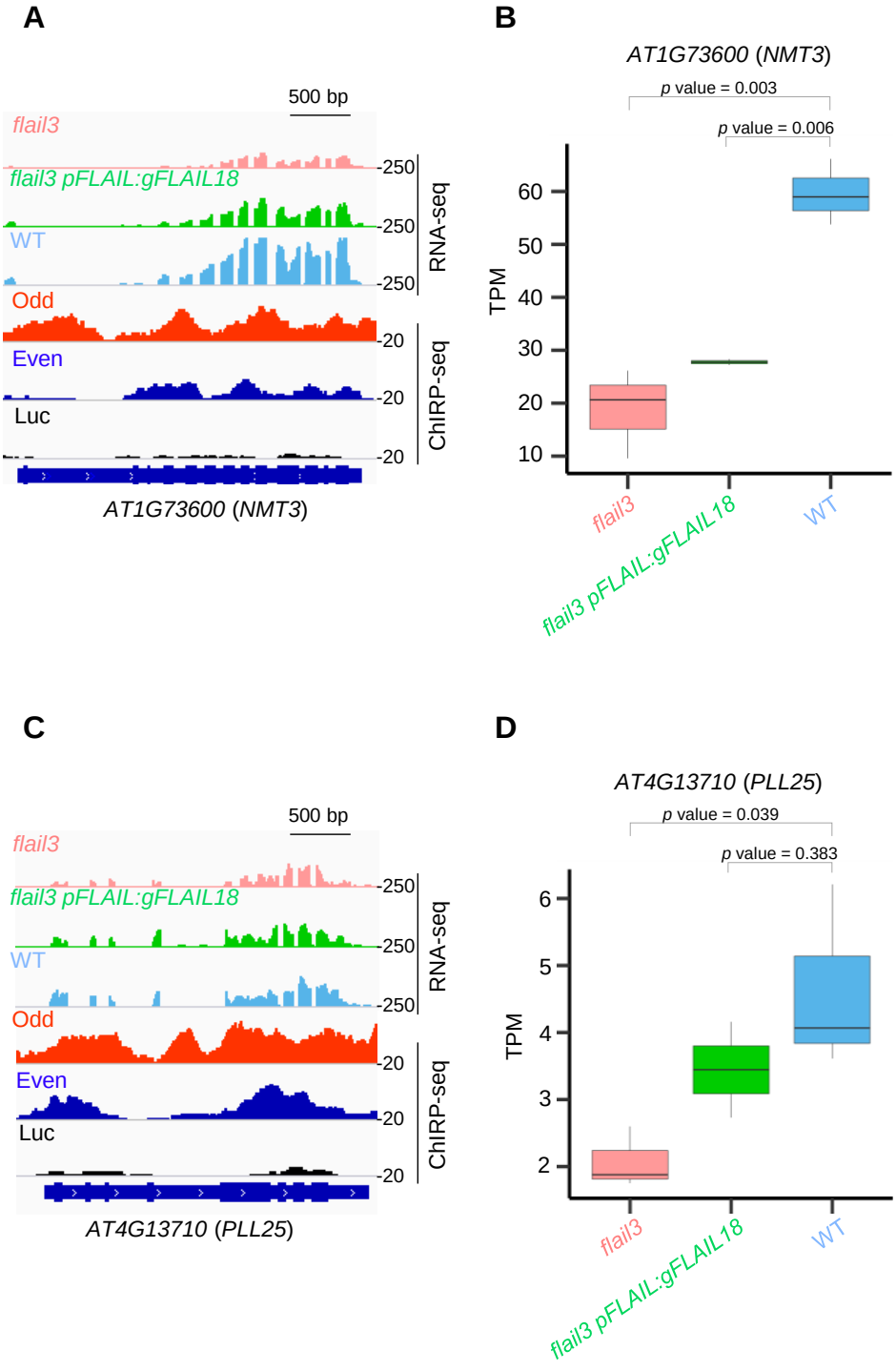

Fig. S9 *FLAIL* binds chromatin regions of flowering genes for gene regulation. **A, C** Genome browser screenshots illustrating two more *FLAIL* bound flowering targets *PLL25* and *NMT3* in RNA-seq (lane 1-3) and ChIRP-seq (lane 4-6). Their expression that was downregulated in *flail3* (lane 1) can be partially or fully rescued in complementation line (lane 2). Both Odd and Even probes identified chromatin binding regions of *FLAIL* in two more flowering genes *NMT3* and *PLL25* compared to *Luc* probes. *FLAIL* binding peaks were called by CCAT3.0. **B, D** Normalized read counts (TPM from RNA-seq) for differentially expressed (DE) flowering genes in WT, *flail3*, and *flail3 pFLAIL:gFLAIL18* plants (bottom panel). Boxes spanned the first to third quartile, bold black lines indicated median value for each group and whiskers represented the minimum and maximum values. *p* value was denoted by Students' t-test.

Fig. S10

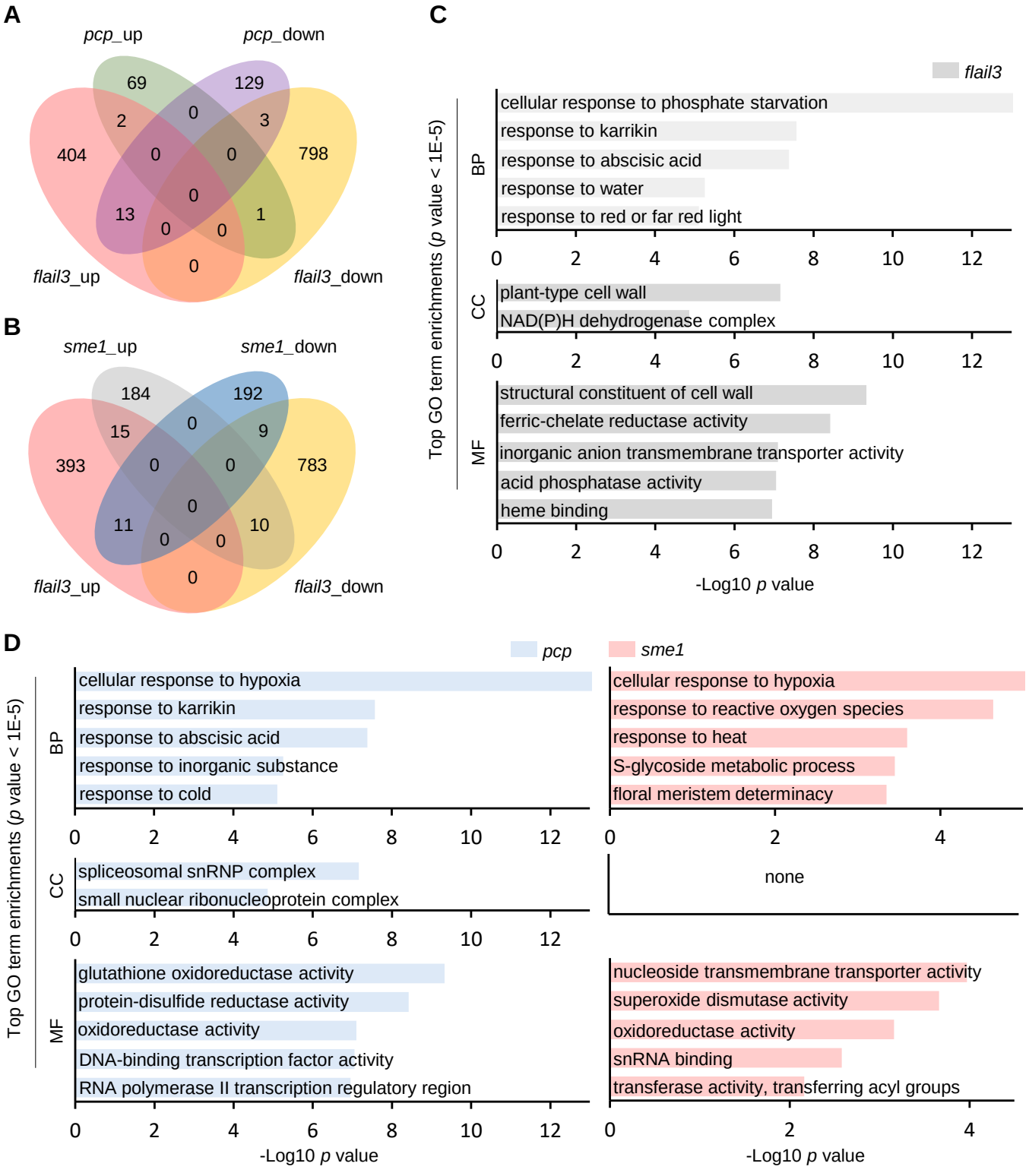

Fig. S10 *FLAIL* regulates flowering independent of *PCP.* **A, B** Venn diagram showing overlapping differentially expressed genes (up/down) sets between *flail3* and *pcp* (also called *sme1*) mutants. **C, D** GO analysis of the DEGs in RNA-seq data of *flail3* and *pcp /sme1* mutants. Y-axis indicated the GO categories including biological process (BP), cellular component (CC) and molecular function (MF); X-axis showed -Log10 *p* value with the cutoff 0.05. Highly enriched GO terms of dysregulated mRNAs analyzed by the Metascape with 5 top enrichment scores.